Permeation and Gating Properties of the L-Type Calcium Channel in Mouse Pancreatic β Cells

PAUL A. SMITH, FRANCES M. ASHCROFT, and CLARE M. S. FEWTRELL

From the University Laboratory of Physiology, Oxford, OX1 3PT, United Kingdom

ABSTRACT Ba^{2+} currents through L-type Ca^{2+} channels were recorded from cell-attached patches on mouse pancreatic β cells. In 10 mM Ba^{2+}, single-channel currents were recorded at −70 mV, the β cell resting membrane potential. This suggests that Ca^{2+} influx at negative membrane potentials may contribute to the resting intracellular Ca^{2+} concentration and thus to basal insulin release. Increasing external Ba^{2+} increased the single-channel current amplitude and shifted the current–voltage relation to more positive potentials. This voltage shift could be modeled by assuming that divalent cations both screen and bind to surface charges located at the channel mouth. The single-channel conductance was related to the bulk Ba^{2+} concentration by a Langmuir isotherm with a dissociation constant ($K_{d(\gamma)}$) of 5.5 mM and a maximum single-channel conductance (γ_{max}) of 22 pS. A closer fit to the data was obtained when the barium concentration at the membrane surface was used ($K_{d(\gamma)}$ = 200 mM and γ_{max} = 47 pS), which suggests that saturation of the concentration–conductance curve may be due to saturation of the surface Ba^{2+} concentration. Increasing external Ba^{2+} also shifted the voltage dependence of ensemble currents to positive potentials, consistent with Ba^{2+} screening and binding to membrane surface charge associated with gating. Ensemble currents recorded with 10 mM Ca^{2+} activated at more positive potentials than in 10 mM Ba^{2+}, suggesting that external Ca^{2+} binds more tightly to membrane surface charge associated with gating. The perforated-patch technique was used to record whole-cell currents flowing through L-type Ca^{2+} channels. Inward currents in 10 mM Ba^{2+} had a similar voltage dependence to those recorded at a physiological Ca^{2+} concentration (2.6 mM). BAY-K 8644 (1 μM) increased the amplitude of the ensemble and whole-cell currents but did not alter their voltage dependence. Our results suggest that the high divalent cation solutions usually used to record single L-type Ca^{2+} channel activity produce a positive shift in the voltage dependence of activation (~32 mV in 100 mM Ba^{2+}).

Address correspondence to Dr. F. M. Ashcroft, University Laboratory of Physiology, Parks Road, Oxford, OX1 3PT, UK.

Clare Fewtrell's permanent address is Department of Pharmacology, Cornell University, Ithaca, NY 14853.

J. GEN. PHYSIOL. © The Rockefeller University Press · 0022-1295/93/05/0767/31 $2.00
Volume 101 May 1993 767–797

INTRODUCTION

Pancreatic β cells secrete insulin in response to glucose. Associated with this secretion is a characteristic pattern of electrical activity that consists of rhythmical oscillations in membrane potential between a hyperpolarized potential and a depolarized plateau upon which bursts of calcium-dependent action potentials are superimposed (see review by Henquin and Meissner, 1984). There is good evidence that Ca^{2+} influx during the action potential (and possibly also the plateau phase) is essential for insulin secretion (reviewed by Prentki and Matschinsky, 1987). β cells from all species thus far investigated possess voltage-gated dihydropyridine-sensitive calcium channels (for review see Ashcroft and Rorsman, 1989) that belong to the L-type family (for nomenclature see Fox, Nowycky, and Tsien, 1987). However, unlike rat β cells (Ashcroft, Kelly, and Smith, 1990; Sala and Matteson, 1990), mouse β cells do not appear to possess T-type calcium channels (Rorsman, Ashcroft, and Trube, 1988; Smith, Rorsman, and Ashcroft, 1989). Mouse β cells thus provide a preparation in which L-type Ca^{2+} channels may be studied in isolation.

In all single-channel studies of β cell L-type Ca^{2+} channels to date, the pipette (extracellular) solution has contained a high concentration of Ba^{2+} (100 mM) to increase the single-channel current amplitude, and the dihydropyridine agonist BAY-K 8644 was included in the bath solution to prolong the channel lifetime (Smith et al., 1989). These conditions, however, produce a poorly defined shift in the voltage dependence of channel gating and permeation. First, the high concentration of barium ions may be expected to screen negative surface charge on the membrane and so shift the voltage dependence of gating to more depolarized potentials; second, BAY-K 8644 has been reported to shift the voltage dependence of L-type calcium channel activation toward more hyperpolarized potentials (Fox et al., 1987; Markwardt and Nilius, 1988; Rorsman et al., 1988). The overall effect is thus to produce an unknown shift in the voltage dependence of calcium channel activation, thereby precluding estimation of the voltage-dependent properties of the Ca^{2+} channel under physiological conditions ($\sim$2.6 mM Ca^{2+} and no BAY-K 8644).

The perforated-patch configuration of the patch-clamp technique (Horn and Marty, 1988) has already been used to measure whole-cell calcium currents (Korn and Horn, 1989; Smith et al., 1989). In this paper, we have used both the perforated-patch and cell-attached configurations of the patch-clamp technique to measure the voltage shifts in permeation and gating of the L-type calcium channel produced by BAY-K 8644, barium, calcium, and sodium in mouse pancreatic β cells.

METHODS

Cell Culture

Single β cells were isolated from the pancreases of NMRI mice (3 mo or older; Bantman & Kingston, Hull, UK, and Oxford Physiology colony). Pancreases were digested with collagenase (type V; Sigma Chemical Co., St. Louis, MO). Individual islets of Langerhans were then hand-picked and subsequently dispersed into single β cells by trituration in a divalent cation-free Hank's solution containing 0.5 mM EDTA and 0.5 mg/ml trypsin (Sigma Chemical Co.). Trypsinization was halted by the addition of tissue culture medium (see below) and the cells were washed and centrifuged several times before plating onto 35-mm plastic culture

dishes (Falcon 3001; Becton Dickinson Microbiology Systems, Cockeysville, MD). The cells were cultured in RPMI 1640 medium supplemented with 11 mM glucose, 10% (vol/vol) heat-inactivated fetal calf serum (GIBCO, BRL, Gaithersburg, MD), and gentamycin (50 μg/ml; GIBCO BRL), and used within 4 d of plating.

Solutions

The composition of the saline solutions is shown in Table I. A 1 mM stock solution of the dihydropyridine agonist BAY-K 8644 was made in dimethylsulfoxide (DMSO) and added to the bath solution as required. DMSO at the concentrations used had no effect on its own.

For cell-attached patch experiments, the pipette solution contained 10 mM tetraethylammonium chloride (TEACl) to block residual potassium channel activity (Bokvist, Rorsman, and Smith, 1990*a*, *b*). Different Ba^{2+} concentrations were obtained by mixing appropriate amounts of the 100 mM Ba^{2+} and 150 mM Na^+ pipette solutions: in the divalent cation-free experiments, the 150 mM Na^+ pipette solution was supplemented with 2 mM EDTA to chelate

TABLE I

Composition of the Saline Solutions

	NaCl	KCl	$MgCl_2$	Cs_2SO_4	K_2SO_4	$CaCl_2$	$BaCl_2$	TEA	HEPES
				mM					
Bath solutions									
High K^+	10	115	1.1	—	—	1*	—	—	10
2.6 mM Ca^{2+}	138	5.6	1.1	—	—	2.6	—	10	10
10 mM Ba^{2+}	128	5.6	1.1	—	—	—	10	10	10
Pipette solutions									
150 mM Na^+‡	150	—	—	—	—	—	—	10	10
100 mM Ba^{2+}	—	—	—	—	—	—	100	10	10
10 mM Ca^{2+}	135	—	—	—	—	10	—	10	10
Cs^+ nystatin§	10	10	7	70	—	—	—	—	10
K^+ nystatin§	10	10	7	—	70	—	—	—	10

All solutions were adjusted to pH 7.4 and had osmolalities ranging from 0.27 to 0.3 osmol.

*10 mM K-EGTA was present to buffer the free calcium to ~80 nM.

‡2 mM EDTA was present to sequester residual divalent cations.

§40 mM sucrose was added to the pipette solutions used in the perforated-patch experiments to increase the osmotic strength. Nystatin was also added to these solutions as detailed in the text.

residual divalent cations (see Hess, Lansman, and Tsien, 1986). A 10 mM Ca^{2+} pipette solution was used in some cases. To control the β cell resting potential in cell-attached experiments, the cells were bathed in high K^+ bath solution. This solution also contained BAY-K 8644 (0.1–1 μM) to facilitate the measurement of single Ca^{2+} channel currents, and 20 mM glucose to increase Ca^{2+} channel activity (Smith et al., 1989).

For perforated patch experiments the bath contained either a 2.6 mM Ca^{2+} or a 10 mM Ba^{2+} bath solution (Table I). Tolbutamide (0.1–0.2 mM) and TEACl (10–20 mM) were added to block ATP-sensitive K currents and residual delayed rectifier K currents, respectively (Bokvist et al., 1990*a*, *b*). In most cases the pipette solution contained Cs^+ (rather than K^+) to reduce outward K^+ currents. 2 mM glutathione was added to chelate any silver ions released from the Ag^+/AgCl electrode. Its high molecular weight (307) suggests that glutathione is unlikely to permeate nystatin pores.

All experiments were carried out at room temperature (21–25°C).

Patch-Clamp Pipettes

These were pulled from borosilicate glass (Hilgenberg, Malsfeld, Germany, or Boralex, Rochester Scientific, Rochester, NY), coated close to their tips with Sylgard (Dow Corning Corp., Midland, MI) to reduce their electrical capacitance, and fire-polished immediately before use. Pipette resistances were typically between 2 and 5 MΩ.

Cell-attached Patch Configuration

For cell-attached patch recording, β cells were bathed in a high K^+ solution which almost completely depolarized the cells. The extent of this depolarization was measured under current clamp in a separate series of experiments, using the perforated-patch technique and a K^+ nystatin solution in the pipette (Table I). The measured resting potential was +5 ± 1.3 mV (range −2 to +9 mV; $n = 8$), which agrees closely with the K^+ equilibrium potential estimated assuming an intracellular potassium concentration of 114 mM (Smith, 1988). As there may be an error in the measured value of the resting potential due to a small Donnan potential across the patch (Horn and Marty, 1988), we have assumed that the resting potential was 0 mV; i.e., that the membrane potential was the inverse of the applied pipette potential.

In most cases, channel activity was elicited by 225–250-ms voltage pulses from a holding potential of −70 or −100 mV. Pulses were applied at a frequency of 0.5 Hz. In high barium concentrations, the channel open probability at negative potentials was very low: channels were therefore activated by a 100-ms prepulse to 0 mV, after which the membrane was stepped to the desired test potential and the single-channel current amplitude was measured before the channels had deactivated. This procedure was only used for measuring the single-channel current–voltage relation and not for measuring channel activity.

Perforated Patch Configuration

Whole-cell currents were recorded using the perforated-patch configuration of the patch-clamp technique (Horn and Marty, 1988). In this method, the pore-forming antibiotic, nystatin, is included in the pipette solution. Nystatin incorporates into the membrane patch and produces a low resistance pathway between the pipette and the cell interior. The advantage of this method is that it provides electrical access to the interior of the cell without disruption of the patch membrane. The nystatin pores are relatively impermeable to divalent cations and uncharged molecules >0.8 nm in diameter; anions are only weakly permeable. Intracellular dialysis by the pipette solution of species other than monovalent cations is therefore prevented and Ca^{2+} currents can be maintained for considerably longer than with the conventional whole-cell configuration (Korn and Horn, 1989; Smith et al., 1989).

A stock solution of nystatin in DMSO (50–100 mg/ml) was prepared and stored at −20°C for up to 1 wk. Each day, the stock solution was ultrasonicated for 6 min and then diluted with the pipette solution and sonicated for a further 12 min; the final nystatin concentration was 50–200 μg/ml in 0.1–0.2% DMSO. All nystatin solutions were protected from light, and with this precaution the final nystatin solution remained usable for up to 4 h. The tip of the pipette was first filled with nystatin-free solution by capillary action and the pipette was then backfilled with the nystatin-containing solution.

After obtaining a seal, the holding potential was set at −70 mV and 10-mV test pulses of 10-ms duration were applied to monitor the access resistance. As nystatin incorporated into the patch membrane, the series resistance decreased and a slow capacitative current appeared. With increasing perforation of the patch membrane this capacity transient became larger and faster, until eventually it was possible to compensate the cell capacitance. The mean cell capacitance was 5.1 ± 0.3 pF and the mean series resistance was 35 ± 2 MΩ (range 14–50 MΩ; $n = 33$); cells in which the series resistance was >33 MΩ were not used for analysis. Series

resistance compensation was not used as it led to clamp instability during perfusion. The voltage error due to the presence of a series resistance (< 33 MΩ) may be expected to be small in our experiments (< 8 mV) because the maximum amplitude of the inward currents we recorded was < 250 pA. For each cell, the voltage error was estimated from the measured series resistance; during later analysis, this voltage was added to the applied potential to obtain the correct membrane potential. In fact, the voltage dependences of whole-cell currents from cells with different access resistances were not significantly different.

The holding potential was −70 mV and 250-ms voltage pulses were applied at a frequency of 0.5 Hz.

Liquid Junction Potentials

The reference potential for all experiments was the zero-current potential before the establishment of the seal. Junction potentials were measured by comparing the zero-current pipette potential in each experimental solution against a reference of 150 mM KCl. In these experiments, the pipette contained 150 mM KCl and the test solution was connected to the reference electrode by a 3 M KCl agar bridge. Since the measured junction potentials were small (< 4 mV), we have not corrected for them in these studies.

Data Recording and Analysis

Currents were recorded with an EPC-7 amplifier (List Electronic, Darmstadt, FRG) and acquired on-line using an Axolab-1 interface with pClamp software (Axon Instruments, Inc., Foster City, CA). Currents were amplified and then filtered using an 8-pole Bessel filter (Frequency Devices Inc., Haverhill, MA). Whole-cell currents were filtered at 2.5 kHz (−3 db) and digitized at 5 kHz; currents from cell-attached patches were filtered at 2–2.5 kHz (−3 db) and digitized at 8–10 kHz. Digitized data were analyzed using a combination of pClamp and in-house software.

Unitary current amplitudes were measured individually and these values were confirmed by cross-reference to an all-points amplitude histogram of the sweep, displayed simultaneously. Ensemble currents were constructed by averaging ~20 sweeps. They were then corrected for capacity and leak currents by averaging sweeps that did not contain channels, scaling this average current and then subtracting it from the ensemble current. In some patches we observed an additional type of inward current which had a single-channel slope conductance of 6 pS in 100 mM Ba^{2+} and long-lasting openings, and which showed little voltage dependence. We have not included records showing noticeable activity of this channel when constructing the ensemble currents.

To measure the voltage dependence of activation, the whole-cell currents were corrected for inactivation by fitting the current decay during the pulse by a single exponential. The exponential was extrapolated to the beginning of the voltage step in order to estimate the peak current. Currents were corrected for inactivation in this way at potentials between −30 and +50 mV.

Functions were fitted to the data by minimizing the square of the residuals by a variable-metric free parameter fitting routine. In the case of implicit functions (Grahame's equation, our Eq. 2), Newton's method was implemented to determine the implicit variable. For Eqs. 3 and 11, which had three free parameters, the possibility of more than one unique solution was explored. That is, calculations were run several times with different initial values for all three parameters. In all cases, the final solutions were very similar; the solution chosen was that with the lowest sum of squares (LSS).

Data are given as mean ± SEM, with the number of observations in parentheses. Paired data were tested for significance using either the sign test or the Wilcoxon test; unpaired data were

tested for significance using the Mann-Whitney test. The significance (P) is given in parentheses.

GLOSSARY

$\psi_{o(p)}$	the external surface potential sensed by the ion permeation pathway
$\psi_{i(p)}$	the internal surface potential sensed by the ion permeation pathway
V_s	the voltage shift required to fit the constant field equation to the single-channel current–voltage relation, which is equal to $\psi_{o(p)} - \psi_{i(p)}$
$\sigma_{(p)}$	initial membrane surface charge density associated with the ion permeation pathway
$K_{d(p)}$	the dissociation constant for the binding of the divalent cation to the membrane surface charge associated with the ion permeation pathway
$K_{d(\gamma)}$	the dissociation constant for the ion binding site within the permeation pathway
P_{Ba}	the measured Ba^{2+} permeability
P_{Ba}	the true Ba^{2+} permeability, obtained by correcting for membrane surface charge
$[Ba^{2+}]_o$	the Ba^{2+} concentration in the bulk solution
$[Ba^{2+}]_s$	the Ba^{2+} concentration at the membrane surface
$\psi_{i(g)}$	the internal surface potential sensed by the gating particle
$\psi_{o(g)}$	the external surface potential sensed by the gating particle
$\sigma_{(g)}$	the initial membrane surface charge density associated with gating
$K_{d(g)}$	the dissociation constant for the binding of the divalent cation to the membrane surface charge associated with gating
N	the total number of channels available for activation
P_o	the channel open probability
P_{max}	the maximum probability of the channel opening
NP_{max}	the maximal channel activity
k	the slope factor describing the steepness of voltage dependence of activation
$V_{0.5}$	the voltage at which half-maximal activation occurs
γ	the single-channel conductance
γ_{max}	the maximum single-channel conductance

RESULTS

In this section, we first discuss the permeation properties of the single-channel currents carried by barium, calcium, and sodium. We then consider the effects of these cations, and that of BAY-K 8644, on the gating of the calcium channel.

Permeation of Ba^{2+} through Ca^{2+} Channels

Fig. 1 *A* illustrates barium currents flowing through single Ca^{2+} channels recorded from a cell-attached patch with a pipette containing 100 mM Ba^{2+}. The associated single-channel current–voltage relation (Fig. 1 *B*; see also Fig. 2) shows inward rectification, as expected since intracellular Ca^{2+} is very low. The current–voltage relation was well fit by a modification of the constant field equation which takes into account a surface potential (Goldman-Hodgkin-Katz [GHK] equation: Goldman, 1943; Hodgkin and Katz, 1949; Frankenhaeuser, 1960):

$$i = \frac{-P_{Ba}(zF)^2\,(V - V_s)}{RT} \exp\,(-zFV_s/RT)\,\frac{[Ba^{2+}]_o - [Ba^{2+}]_i \exp\,(zFV/RT)}{1 - \exp\,[zF(V - V_s)/RT]} \qquad (1)$$

where i is the single-channel current and z, F, R, and T have their usual meanings. V

is the membrane potential across the patch (in volts) and V_s is the voltage shift due to the difference between external ($\psi_{o(p)}$) and internal ($\psi_{i(p)}$) surface potentials. $[Ba^{2+}]_o$ and $[Ba^{2+}]_i$ are the bulk extracellular and intracellular Ba^{2+} concentrations (in millimoles), respectively. $[Ba^{2+}]_i$ was assumed to be negligible and was taken as zero: varying $[Ba^{2+}]_i$ between 0 and 0.1 mM was without effect on the fitted relationship. P_{Ba} is the measured (fitted) barium permeability which is related to the true barium permeability (P_{Ba}) by the following equation:

$$P_{Ba} = P_{Ba} \exp(-zF\psi_{i(p)}/RT) \quad (2)$$

The dotted line in Fig. 1 *B* was an attempt to fit the GHK equation assuming no voltage shift ($V_s = 0$) and clearly deviates from the data. Only when a voltage shift was included in the GHK equation, to take account of surface potentials, was a good fit to the single-channel current–voltage relation obtained (Fig. 1 *B*, *solid line*). The mean

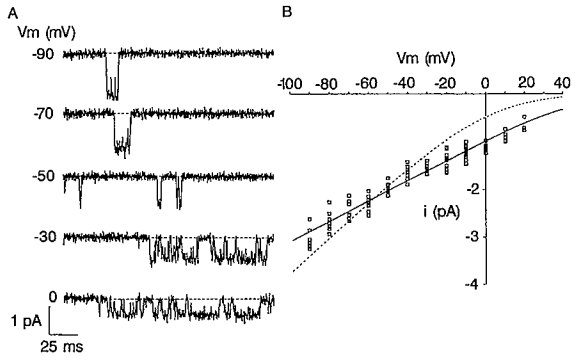

FIGURE 1. (*A*) Single Ca^{2+} channel currents recorded at different pipette potentials with 100 mM Ba^{2+} in the pipette. Channels were activated by a 100-ms prepulse to 0 mV from a holding potential of −70 mV and openings were recorded on returning the membrane to the potentials indicated. At negative potentials, channel openings are clustered toward the beginning of the sweep, accounting for the rapid deactivation of Ca^{2+} tail currents at these potentials (Rorsman and Trube, 1986). Filter frequency, 2 kHz. (*B*) Single-channel current–voltage relationship for the channel shown in *A*. Individual current amplitudes are plotted to demonstrate their variability. The solid line through the data points is the best fit of the GHK equation (Eq. 1) to these data: $P_{Ba} = 5.6 \times 10^{-13}$ cm^3s^{-1} and $V_s = +45$ mV. The dotted line is drawn to Eq. 1 with $P_{Ba} = 0.25 \times 10^{-13}$ cm^3s^{-1} and $V_s = 0$ mV (i.e., without a voltage shift).

value of the voltage shift was +45.0 ± 2.1 mV ($n = 7$) and that of the barium permeability was 5.2 ± 0.7 × 10^{-13} cm^3s^{-1} ($n = 7$). Rorsman et al. (1988) reported that they were only able to satisfactorily fit the standard GHK equation to the single Ca^{2+} channel current–voltage relation measured in outside-out patches from mouse β cells by adding a 30-mV shift to the fitted curve. Using a similar approach, we obtained a barium permeability of 0.15 ± 0.01 × 10^{-13} cm^3s^{-1}, which is close to the 0.13 ± 0.01 × 10^{-13} cm^3s^{-1} they reported (Rorsman et al., 1988). The single-channel slope conductances, measured over the linear range of the current–voltage relation, are also similar: 22 ± 1 pS ($n = 7$) compared with 24 pS in 110 mM Ba^{2+} obtained by Rorsman et al. (1988).

Although assumptions concerning the mechanism of ion permeation are inherent in the use of constant field theory (Goldman, 1943; Hodgkin and Katz, 1949), we were nevertheless able to obtain close fits of the GHK equation to our data at all

barium concentrations used (see below). Barrier models based on Eyring rate theory can provide a more complete description of ion permeation through L-type calcium channels but are considerably more complex (Almers and McCleskey, 1984; Hess and Tsien, 1984; Yue and Marban, 1990). Since our main aim was to relate the channel properties measured in 100 mM barium to those at a physiological calcium concentration (2.6 mM) we have chosen to fit our data using the constant field theory because this has the least number of free parameters.

Voltage shift due to membrane surface charge. To determine the $[Ba^{2+}]_o$ dependence of the voltage shift of the single-channel current–voltage relationship, single-channel currents were recorded in barium concentrations ranging from 5 to 100 mM. Fig. 2 shows channel openings recorded at −30 mV (*A*) and representative current-voltage relationships (*B*) at different barium concentrations. As the barium concentration is decreased, there is both a decrease in the slope of the current–voltage relation and a shift to more negative potentials. These effects combine to produce a

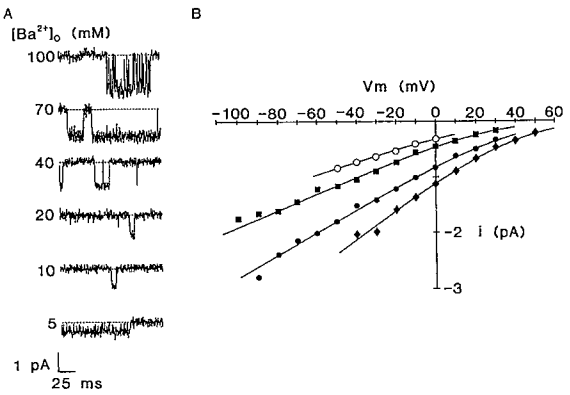

FIGURE 2. (*A*) Single Ca^{2+} channel currents recorded with different barium concentrations in the pipette. Currents were elicited by a voltage step to −30 mV from a holding potential of −70 mV. Filter frequency, 2 kHz. (*B*) Representative single-channel current–voltage relations measured at different barium concentrations. (○) 5 mM Ba^{2+}, (■) 10 mM Ba^{2+}, (●) 40 mM Ba^{2+}, (◆) 100 mM Ba^{2+}. The solid lines are the best fits to Eq. 1 using values of P_{Ba} and V_s of (○) 8.4×10^{-13} cm^3s^{-1} and +22 mV, (■) 8.1×10^{-13} cm^3s^{-1} and +27 mV, (●) 6.6×10^{-13} cm^3s^{-1} and +38 mV, and (◆) 5.1×10^{-13} cm^3s^{-1} and +45 mV, respectively.

marked reduction in the unitary current amplitude at low barium concentrations (Fig. 2 *A*).

The individual values obtained for the voltage shift (V_s, Eq. 1) in each patch are plotted as a function of $[Ba^{2+}]_o$ in Fig. 3 *A*. When $[Ba^{2+}]_o$ is raised, the voltage shift increases, from +15.1 ± 5.6 mV (n = 8) in 5 mM $[Ba^{2+}]_o$ to +45.0 mV ± 2.1 mV (n = 8) in 100 mM $[Ba^{2+}]_o$. This shift can be explained by the combined effects of the divalent cation binding to and screening fixed negative charges on the membrane surface (see below).

V_s varies significantly between patches (Fig. 3 *A*). The increase in the variability of V_s at low $[Ba^{2+}]_o$ (a range of 50 mV in 5 mM barium) may be attributed to the greater difficulty of fitting the single-channel current–voltage relationship when its slope is less steep.

We attempted to fit the barium dependence of the voltage shift using several models. First, we assumed that only specific binding of Ba^{2+} to membrane surface

charge takes place, using the empirical equation given in the figure legend (Fig. 3 *B*; Hagiwara and Takahashi, 1967). This approach does not provide a physical basis to the voltage shift from which membrane surface charge density can be calculated. We have therefore fitted the data with the Grahame equation assuming either: (*a*) that Ba^{2+} only screens membrane surface charges and does not bind (Fig. 3 *C*); or (*b*) that Ba^{2+} both screens and binds to membrane surface charges (Fig. 3 *A*). Like others, we have assumed that both Ba^{2+} and Na^+ can contribute to screening (McLaughlin, Szabo, and Eisenman, 1971; Wilson, Morimoto, Tsuda, and Brown, 1983; Cota and Stefani, 1984; Ganitkevich, Shuba, and Smirnov, 1988). The Grahame equation is:

$$\sigma_f = \frac{1}{2.72}\{\Sigma\,[C_j\,[\exp\,(-z_jF\psi_o/RT) - 1]]\}^{0.5} = \frac{\sigma}{1 + \Sigma\,[K_aC_j\exp\,(-z_jF\psi_o/RT)]} \quad (3)$$

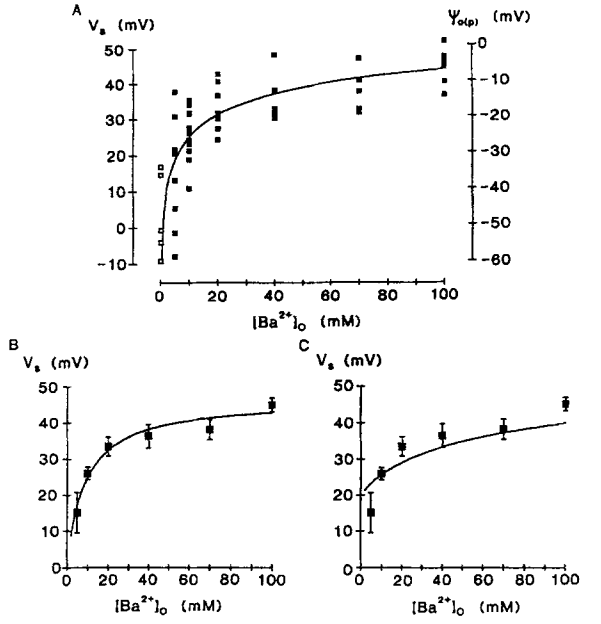

FIGURE 3. (*A*) The effect of the bulk barium concentration ($[Ba^{2+}]_o$, abscissa) on the voltage shift associated with permeation (V_s, left ordinate) and the external surface potential ($\psi_{o(p)}$, right ordinate). Each point represents a different patch. The solid line is fitted to Eq. 3 with $\sigma_{i(p)}$ = 1.4 e.nm^{-2}, $\psi_{i(p)}$ = −51 mV, and $K_{a(p)}$ = 77 M^{-1} (LSS = 3,286). Data at 0 mM $[Ba^{2+}]_o$ (□) were obtained using the 150 mM Na^+ pipette solution (divalent cation free) and were not used in the fit. (*B*) Same data as in *A* given as mean ± SEM which were fit assuming binding only by using the empirical equation $V_s = V_{max}/[1 + (K_d/[Ba^{2+}]_o)]$, where K_d = 9 mM and V_{max} = +47 mV (LSS = 3,686). (*C*) Same data as in *A*, fit assuming screening only. The solid line is fit to Eq. 3 with no binding (i.e., $K_{d(p)} = 0$), where $\sigma_{i(p)}$ = 0.6 e.nm^{-2} and $\psi_{i(p)}$ = −77 mV (LSS = 4,195).

where σ_f is the free surface charge density (in electronic charges per square nanometer; e.nm^{-2}), σ is the initial surface charge density (e.nm^{-2}), ψ_o is the external surface potential, C_j is the concentration of the jth ionic species in the bulk solution, z_j is its valence, and K_a is the association constant for the binding of the divalent cation to the membrane surface charge (monovalent ions are assumed not to bind). The dissociation constant, K_d, is given by $1/K_a$. We use the subscript (p) to refer to the values of σ_i, ψ_i, K_a, and K_d calculated from shifts in ion permeation; below, we use the subscript (g) to refer to the values calculated from the voltage shifts associated with gating.

The external surface potential associated with permeation ($\psi_{o(p)}$) is related to the

measured voltage shift (V_s) by

$$\psi_{o(p)} = \psi_{i(p)} + V_s \tag{4}$$

where $\psi_{i(p)}$ is the surface potential at the internal face of the channel pore associated with permeation. Substituting Eq. 4 into Eq. 3 enables values for the three free parameters $\sigma_{(p)}$, $K_{a(p)}$, and $\psi_{i(p)}$ to be obtained from the best fit of Eq. 3 to the data. We have assumed that $\psi_{i(p)}$ is constant and does not change with external cation concentration. Note that at high barium concentrations the external surface charge is expected to saturate, such that $\psi_{o(p)}$ tends to zero and V_s becomes the inverse of $\psi_{i(p)}$ (i.e., $-\psi_{i(p)}$), and that when the measured voltage shift is zero, $\psi_{o(p)} = \psi_{i(p)}$.

The best fit to the barium dependence of the voltage shift (Fig. 3 *A*) was obtained with a $\sigma_{(p)}$ of 1.4 e.nm^{-2}, a $K_{a(p)}$ of 76.9 M^{-1} for barium (i.e., $K_{d(p)}$ is 13 mM), and a $\psi_{i(p)}$ of −51.1 mV.

Conductance. The single-channel slope conductances (γ), estimated from the linear portions of the current–voltage curves, are plotted in Fig. 4 *A* as a function of barium concentration. The conductance saturates with increasing $[Ba^{2+}]_o$, and thus appears to violate the independence principle that is assumed in fitting the GHK equation. The line drawn through the data in Fig. 4 *A* is the best fit of the data to a Langmuir saturation curve:

$$\gamma = \frac{\gamma_{max}\,[Ba^{2+}]_o}{[Ba^{2+}]_o + K_{d(\gamma)}} \tag{5}$$

where γ_{max}, the maximum single-channel conductance, is 22 pS, and $K_{d(\gamma)}$, the dissociation constant for the ion-binding site within the permeation pathway, is 5.5 mM. Both these values are smaller than those measured for L-type calcium channels in other tissues (30 pS and 13 mM, Rosenberg, Hess, and Tsien, 1988; 26.8 pS and 8 mM, Ganitkevich and Isenberg, 1990).

The presence of a surface potential would mean that the surface barium concentration, $[Ba^{2+}]_s$, will be greater than that in the bulk solution. $[Ba^{2+}]_s$ was therefore estimated from the mean surface potential, $\psi_{o(p)}$, determined at each bulk barium concentration, $[Ba^{2+}]_o$, using the Boltzmann relation (Ganitkevich et al., 1988):

$$[Ba^{2+}]_s = [Ba^{2+}]_o \exp\left(\frac{-zF\psi_{o(p)}}{RT}\right) \tag{6}$$

The slope conductance can be described as a function of the surface barium concentration by using Eq. 5 and substituting $[Ba^{2+}]_o$ for $[Ba^{2+}]_s$. The best fit to this modified equation is shown in Fig. 4 *B* and gave values of 47 pS for γ_{max} and 200 mM for $K_{d(\gamma)}$. This fit provides a much better description of the data than that shown in Fig. 4 *A*, where bulk barium concentrations were used.

When the slope conductance was plotted as a function of $[Ba^{2+}]_s$ rather than $[Ba^{2+}]_o$, it is clear that there is much less saturation (Fig. 4 *C*). This observation has implications for models of ion permeation through the L-type calcium channel. It demonstrates that constant field theory provides a far better description of ion permeation through the Ca channel than is generally recognized; this is because saturation of the conductance–concentration relation results largely from the satura-

tion of membrane surface charges that concentrate cations in the vicinity of the channel mouth rather than from ion binding within the pore. Clearly, an overestimate of the affinity of ion-binding sites within the pore will occur if the ability of membrane surface charge to increase the local cation concentration is ignored.

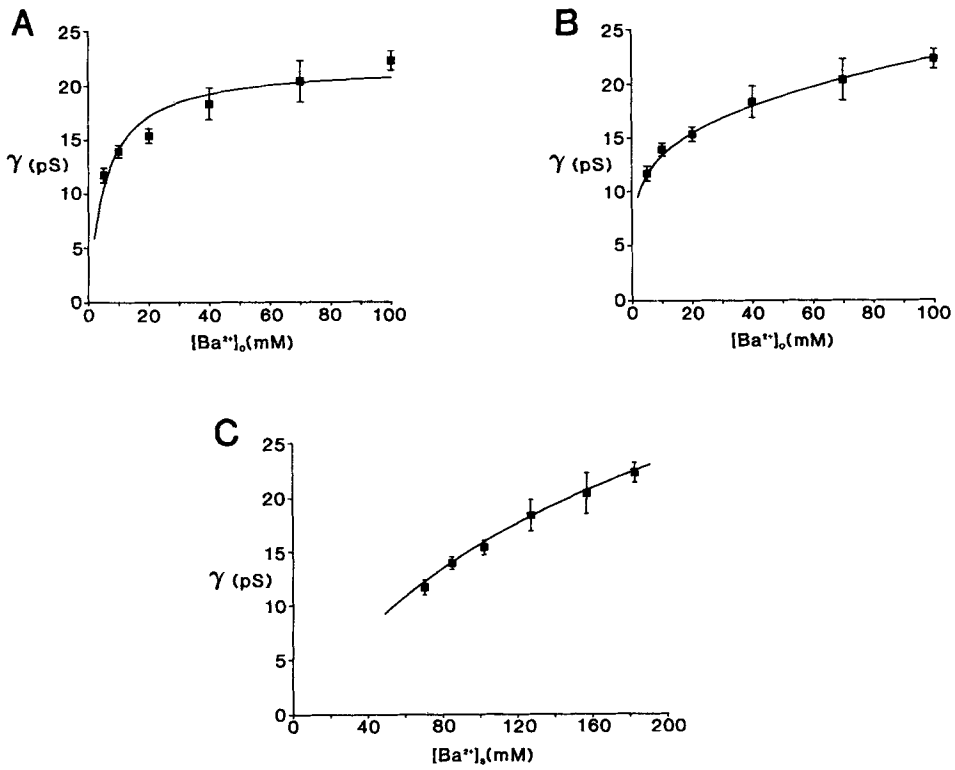

FIGURE 4. (*A*) Relationship between the single-channel slope conductance (γ, ordinate) and the bulk barium concentration (abscissa, $[Ba^{2+}]_o$). Data points show the mean ± SEM of 5–14 patches at each barium concentration. The line is the best fit to Eq. 5 using the values given in the text. (*B*) Relationship between the single-channel slope conductance (γ, ordinate) and the bulk barium concentration (abscissa, $[Ba^{2+}]_o$). The data points are the same as in *A*, but the line is the best fit to Eq. 5 using surface barium concentrations calculated from Eq. 6. (*C*) Relationship between the single-channel slope conductance (γ, ordinate) and the surface barium concentration (abscissa, $[Ba^{2+}]_s$). The line is the best fit to Eq. 5 using surface barium concentrations calculated from Eq. 6. Data are the same as in *A*.

Permeation of Ca^{2+} through Ca^{2+} Channels

Fig. 5 illustrates channel openings elicited at −30 mV with either 10 mM Ca^{2+} (*A*) or 10 mM Ba^{2+} (*B*) in the pipette. Ca^{2+} currents are of smaller amplitude than Ba^{2+} currents (−0.3 and −0.8 pA at −30 mV, respectively), indicative of a lower Ca^{2+} permeability. The channel kinetics are also different, the open times being shorter when calcium carries current. Although not obvious in Fig. 5 *A*, in general we noticed

that Ca^{2+} currents tended to be clustered toward the beginning of the trace, especially at positive potentials. This produces an ensemble current that inactivates more rapidly (see Fig. 6 *B*).

Fig. 5 *C* shows the single-channel current–voltage relations in 10 mM $[Ca^{2+}]_o$ and 10 mM $[Ba^{2+}]_o$. In 10 mM Ca^{2+} the mean permeability was $3.6 \pm 1.2 \times 10^{-13}$ cm^3s^{-1} ($n = 14$) and the slope conductance was 6.6 ± 0.5 pS ($n = 14$), values that are about half those measured in 10 mM barium ($P_{Ba} = 7.7 \pm 1 \times 10^{-13}$ cm^3s^{-1} and $\gamma = 13.9 \pm 0.5$ pS; $n = 14$), suggesting that Ba^{2+} is more permeable than Ca^{2+}. The voltage shift, V_s, was similar in the two solutions, being 22 ± 4 mV ($n = 14$) in Ca^{2+}

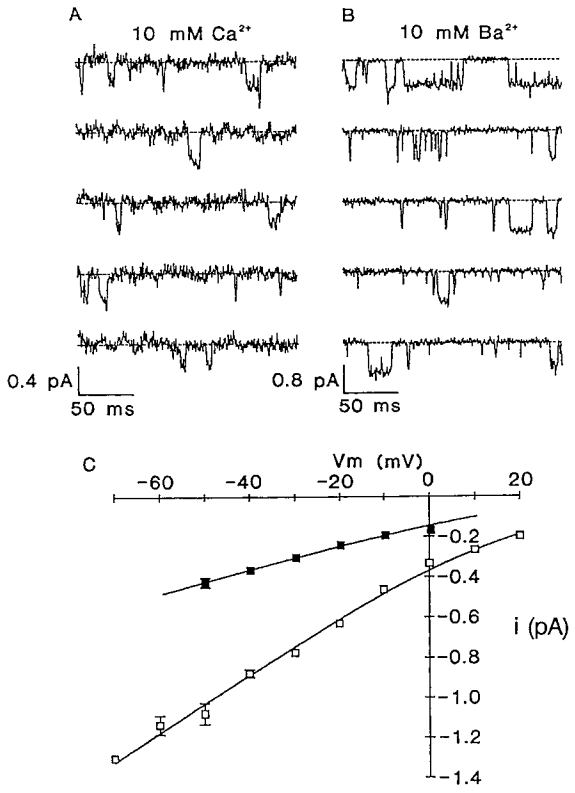

FIGURE 5. Single Ca^{2+} channel currents recorded with 10 mM Ca^{2+} (*A*) or 10 mM Ba^{2+} (*B*) in the pipette. Currents were elicited by a 250-ms step to −30 mV from a holding potential of −100 mV. Filter frequency 0.5 kHz. (*C*) Associated single-channel current–voltage relationship recorded with 10 mM Ca^{2+} (■) or 10 mM Ba^{2+} (□). Lines are best fits of the data to Eq. 1 with $P_{Ca} = 0.43 \times 10^{-13}$ cm^3s^{-1} and $V_s = +21$ mV (■) and with $P_{Ba} = 1.0 \times 10^{-13}$ cm^3s^{-1} and $V_s = +19$ mV (□).

and 26 ± 2 mV ($n = 14$) in Ba^{2+} (Table II). If we assume that both the initial surface charge density ($\sigma_{(p)}$) and the internal surface potential ($\psi_{i(p)}$) associated with the permeation pathway are the same in the barium and calcium solution, it is possible to estimate the dissociation constant for calcium ($K_{d(p)}$) from Eq. 3. Using the measured value of V_s (22 mV) and taking $\sigma_{(p)}$ as 1.4 $e.nm^{-2}$ and $\psi_{i(p)}$ as −51.1 mV, we found $K_{d(p)}$ to be 18.3 mM. The comparable value for barium is 13 mM (Table II).

Although we were unable to measure single-channel currents in 2.6 mM Ca^{2+}, it is possible to estimate their properties if we assume that the Ca^{2+} permeability is unaltered between 2.6 and 10 mM Ca^{2+}. With this condition, we obtained a value of

+10 mV for V_s and −0.3 pA for the single-channel current amplitude at −70 mV in 2.6 mM Ca^{2+} at 20°C.

Voltage Dependence of Ca^{2+} Channel Gating: Ensemble Ba^{2+} Currents

In 10 mM barium, channel openings were regularly observed at the holding potential of −70 mV, which is close to the normal resting potential of the β cell. Occasional openings were even seen at holding potentials as negative as −120 mV. Openings of L-type calcium channels at very negative membrane potentials have also been observed in cardiac myocytes under similar recording conditions (Ganitkevich and Isenberg, 1990).

At high (100 mM) barium concentrations, channel activity was normally only observed at membrane potentials positive to −50 mV (Smith et al., 1989). This shift in the voltage dependence of channel activation probably arises from barium screening and/or binding to membrane surface charge within the vicinity of the

TABLE II

Comparison of Permeation and Gating Parameters

	V_s	$K_{d(p)}$	$[X]_{s(p)}$	P_x	P_x	γ	$V_{0.5}$	$K_{d(g)}$	k
	mV	*mM*	*mM*	*×10⁻¹³ cm³s⁻¹*		*pS*	*mV*	*mM*	*mV*
Single-channel currents									
10 mM Ba^{2+}	26.0 ± 1.7	13*	70	7.7 ± 1.0	0.15‡	13.9 ± 0.6	−23.1 ± 1.6	430	7.9 ± 0.5*
10 mM Ca^{2+}	22.4 ± 3.6	18.3‡	92	3.6 ± 1.2	0.07‡	6.6 ± 0.5	−3.1 ± 2.0	38§	8.2 ± 1.0
150 mM Na^+	3.6 ± 5.5	336‡	980	1.0 ± 0.2	0.14‡	43.0 ± 3.0	−44.4 ± 3.6	∞	7.5 ± 1.1
Whole-cell currents									
10 mM Ba^{2+}	4.5 ± 5.0	—	—	—	—	—	3.5 ± 1.9	—	7.6 ± 0.3
2.6 mM Ca^{2+}	−7.0 ± 2.0	—	—	—	—	—	−3.8 ± 1.3	—	8.4 ± 0.6

$[X]_{s(p)}$ is the surface concentration of the ion X associated with the permeation pathway, calculated from Eq. 6. *For all Ba^{2+} concentrations. ‡Determined using the values of 1.4 e.nm^{-2} for $\sigma_{i(p)}$ and −51.1 mV for $\psi_{i(p)}$ obtained from analysis of single-channel Ba^{2+} currents. §Determined using the values of 0.54 e.nm^{-2} for $\sigma_{i(g)}$ and −20 mV for $(B - \psi_{i(g)})$ obtained from analysis of ensemble Ba^{2+} currents.

gating particle(s). To test this idea, ensemble currents were constructed by averaging single-channel currents recorded at each potential. These average currents were then plotted as a function of membrane potential to determine the voltage dependence of activation and the voltage at which the maximal current occurred. Ensemble currents recorded in 10 mM Ba^{2+} are shown in Fig. 6 *A*. In some patches, the ensemble Ba^{2+} currents inactivated at potentials positive to +10 mV. This is not likely to be due to activation of an outward current because the individual traces showed greater single-channel activity at the beginning of the trace and no outward single-channel currents were observed (data not shown). When calcium was the charge carrier, inactivation of the ensemble currents was faster and more complete during a voltage step of similar length (Fig. 6 *B*).

Representative peak ensemble current–voltage relationships in 10 and 40 mM barium are shown in Fig. 7 *A* and resemble the whole-cell barium currents (see Figs. 10 and 14). The current–voltage relation is shifted toward more positive potentials at

the higher Ba^{2+} concentration. This is presumably due to an increase in the screening of (and binding to) negative surface charge by the divalent cation, as previously described for whole-cell calcium currents (Wilson et al., 1983; Cota and Stefani, 1984; Ganitkevich et al., 1988).

The ensemble current amplitude (I) is given by:

$$I = NP_o i \tag{7}$$

where N is the number of channels available for activation, P_o is the channel open probability, and i is the single-channel current amplitude. Peak channel activity (NP_o)

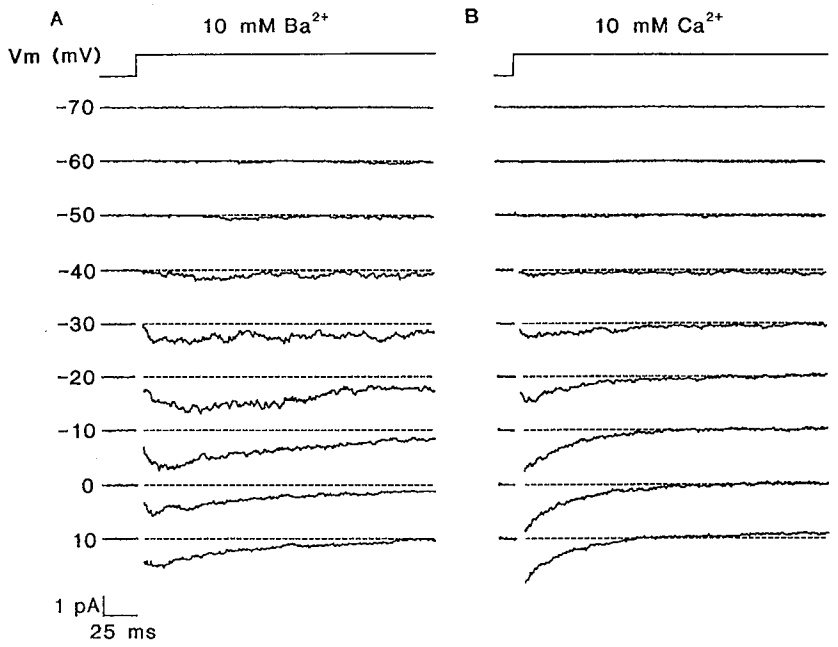

FIGURE 6. Ensemble average currents, 20 sweeps, recorded with 10 mM Ba^{2+} (*A*) and 10 mM Ca^{2+} (*B*). Currents were elicited by a 200-ms step to potentials indicated from a holding potential of −100 mV. The pulse protocol is indicated above. Filter frequency 0.5 kHz. Capacity transients have been removed for clarity.

for each potential was obtained by dividing the peak ensemble current by the single-channel current amplitude determined at the same potential and in the same patch (from the fit to Eq. 1). We were able to calculate the voltage dependence of NP_o in a number of patches which had substantial channel activity (Fig. 7 *B* and 12 other patches). It was not possible, however, to correct satisfactorily for the presence of a developing outward current at more positive potentials and these values have therefore been excluded from the analysis.

The Boltzmann relationship was used to describe NP_o as a function of voltage (see

also Atwell and Eisner, 1978):

$$NP_o = \frac{NP_{max}}{\{1 + \exp[-(V - V_{0.5})/k]\}^n} \quad (8)$$

where $V_{0.5}$ is the voltage at which half-maximal activation occurs, k is the slope factor, and n is the reaction order, which was fixed at 1. N is the total number of channels available for activation and P_o is the probability of the channel opening; as a change

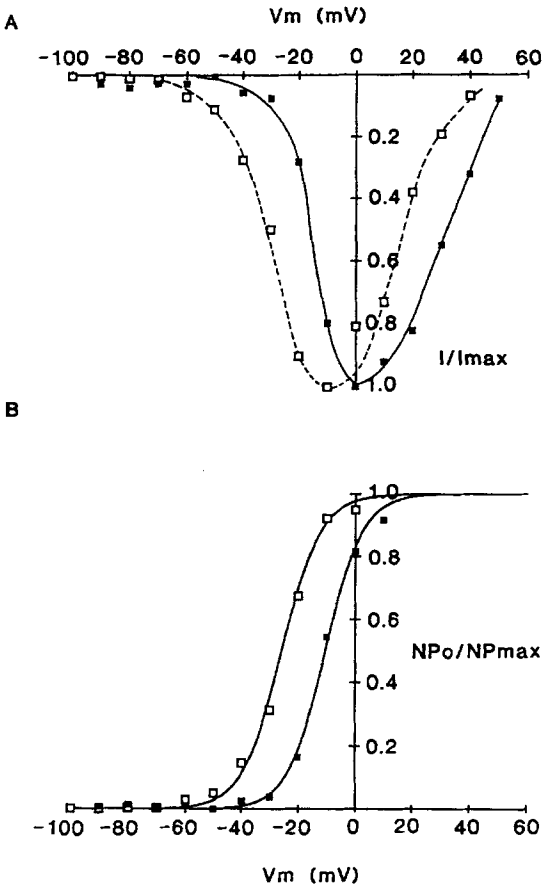

FIGURE 7. (*A*) Representative peak ensemble current–voltage relationship recorded in 10 mM Ba^{2+} (□) and for a different patch with 40 mM Ba^{2+} (■). Currents have been normalized to the maximum value measured. (*B*) Normalized channel activity (NP_o/NP_{max}) as a function of membrane potential (V_m) in 10 mM (□) and 40 mM (■) Ba^{2+}. The lines are fit to Eq. 8 using the parameters given in the text. Same data as in *A*.

in N cannot be distinguished from a change in P_o, we have lumped them together as NP_o, the channel activity. For the examples shown in Fig. 7 *B*, k is +7.5 and +6.5 mV, and $V_{0.5}$ is −25 and −11 mV in 10 and 40 mM barium, respectively. Although a second-order reaction (i.e., $n = 2$) may be more appropriate for voltage-dependent activation of L-type calcium channels (Markwardt and Nilius, 1988; Cena, Stutzin, and Rojas, 1989), we found that a first-order reaction ($n = 1$) gave just as good a fit to our data. The value of k obtained from the ensemble currents was independent of both the concentration and species of permeant ion; the mean value for all Ba^{2+}

concentrations was +7.9 ± 0.5 mV (n = 15) and for 10 mM Ca^{2+} was +8.2 ± 1.0 mV (n = 6).

In over half of the patches in which barium was used as the charge carrier (14 of 27), channel activity was so low that only the voltage at which the maximum current occurred, V_{max}, could be determined with accuracy. It is possible to estimate $V_{0.5}$ from V_{max} if k, γ, and the single-channel current amplitude (i) at V_{max} are known. Thus:

$$V_{0.5} = V_{max} - k \ln\{[-i/(k\gamma)] - 1\} \quad (9)$$

k was taken as 8 mV (see above). The values of $V_{0.5}$ obtained using Eq. 9 were very similar to those derived from fitting Eq. 8 to the voltage dependence of NP_o in patches showing high channel activity. The mean difference in the measured and estimated values was 0.92 ± 1.33 mV (n = 12; t = −0.7; P = 0.51; paired t test) and lay within the range of experimental error.

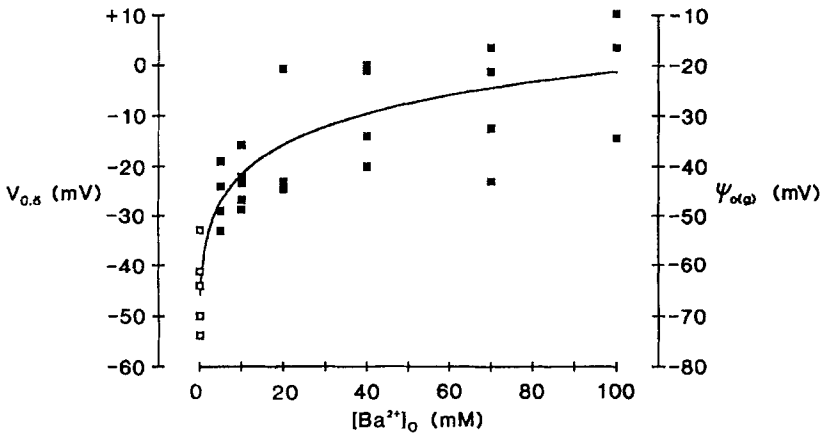

FIGURE 8. Relationship between the bulk barium concentration (abscissa, $[Ba^{2+}]_o$) and the voltage at which NP_o was half-maximal ($V_{0.5}$, left ordinate) and the external surface potential (right ordinate, $\psi_{o(g)}$). Each data point was obtained from a different patch. The line is the best fit to Eq. 3 with a $\sigma_{i(g)}$ of 0.54 e.nm^{-2}, a ($B - \psi_{i(g)}$) of −20 mV, and a $K_{d(g)}$ of 430 mM. Data at 0 mM $[Ba^{2+}]_o$ (□) were obtained using the 150 mM Na^+ pipette solution (divalent cation free) and were not included in the fit.

In Fig. 8, $V_{0.5}$ is plotted as a function of the bulk barium concentration. Although the data are scattered, $V_{0.5}$ clearly shifts toward more positive potentials as the barium concentration increases, and saturates toward the higher concentrations.

The shift in the voltage dependence of activation was fitted by assuming that barium both screens and binds to the membrane surface charge associated with channel gating (Eq. 3). In this case:

$$V_{0.5} = \psi_{o(g)} - \psi_{i(g)} + B \quad (10)$$

where $\psi_{i(g)}$ is the internal and $\psi_{o(g)}$ the external surface potential associated with gating. $V_{0.5}$ is the voltage at which channel activation is half-maximal and B is the potential at which half-maximal activation would occur in the absence of any surface

potential. We assume that both B and $\psi_{i(g)}$ are constant and independent of the experimental conditions (Wilson et al., 1983), and lump them together as $(B - \psi_{i(g)})$.

The solid line in Fig. 8 was obtained by substituting Eq. 10 into Eq. 3 and fitting the resulting expression to the data (the data obtained in divalent cation-free solution were excluded from this fit). The best fit gave values of -20 mV for $(B - \psi_{i(g)})$, of 0.54 e.nm^{-2} for $\sigma_{(g)}$ (the initial surface charge density associated with gating), and of 430 mM for $K_{d(g)}$ (the Ba^{2+} dissociation constant associated with gating). We also fitted the Grahame equation (Eqs. 3 and 10) to the data obtained from those 14 patches in which we were able to measure $V_{0.5}$ directly (from Eq. 8), with similar results: -17 mV for $(B - \psi_{o(g)})$, 0.45 e.nm^{-2} for $\sigma_{(g)}$, and 430 mM for $K_{d(g)}$. Both these sets of values differ markedly from those associated with permeation determined from the same patches ($\psi_{i(p)} = -52.4$ mV, $\sigma_{(p)} = 1.8$ e.nm^{-2}, $K_{d(p)} = 8$ mM). This suggests that membrane surface charge associated with channel gating is quite different from that associated with ion permeation: the gating domain appears to possess a lower initial charge density and a lower binding affinity.

The relationship between $V_{0.5}$ and V_s (the voltage shift measured for permeation) for a number of different patches is shown in Fig. 9 *A*. The individual data points are too scattered to be certain whether or not there is a correlation between the value of $V_{0.5}$ and that of V_s in the same patch, although a plot of the mean value of $V_{0.5}$ against the mean value of V_s for each Ba^{2+} concentration (Fig. 9 *B*) suggests that a relationship between these two parameters may exist.

Voltage Dependence of Ca^{2+} Channel Gating: Ensemble Ca^{2+} Currents

Ensemble currents recorded in 10 mM Ca^{2+} are shown in Fig. 6 *B*. In the majority of patches, a slowly activating outward current developed at potentials positive to +10 mV, which may be expected to cause a small but significant error in the peak amplitude of the ensemble current. The ionic basis of this outward current was not investigated, but it is likely that it is blocked by Ba^{2+} since outward currents were larger in calcium solutions.

The peak ensemble current was largest at $+5 \pm 1$ mV ($n = 7$) in 10 mM Ca^{2+} currents and at -12 ± 1 mV ($n = 7$) in 10 mM $[Ba^{2+}]_o$. From Eq. 9, we calculate $V_{0.5}$ to be -3.1 ± 2 mV ($n = 7$) in 10 mM $[Ca^{2+}]_o$ and -23 ± 2 mV ($n = 7$) in 10 mM $[Ba^{2+}]_o$, taking k as 8 mV in both cases. If we assume that $(B - \psi_{i(g)})$ and $\sigma_{(g)}$ are independent of the cation, and use the values of -20 mV for $(B - \psi_{i(g)})$ and of 0.54 e.nm^{-2} for $\sigma_{(g)}$ obtained for barium, we calculate the Ca^{2+} dissociation constant, $K_{d(g)}$, as 38 mM. This is smaller than that found for barium (430 mM; Table II), implying that surface charge associated with channel gating has a much higher affinity for Ca^{2+} than for Ba^{2+}. Assuming that magnesium does not bind to this surface charge, we estimate that at the physiological Ca^{2+} concentration of 2.6 mM the whole-cell current would be maximal at about -5 mV and the activation curve would be half-maximal at -15 mV. These values are ~ 7 mV more positive than those measured in 10 mM Ba^{2+} (maximum current at -12 mV and $V_{0.5} = -23$ mV).

Voltage Dependence of Ca^{2+} Channel Gating: Whole-Cell Currents

The relatively low probability of Ca^{2+} channel opening hinders an accurate estimation of the voltage dependence of channel gating from the ensemble currents. We

therefore used the perforated-patch technique to record whole-cell currents flowing through calcium channels. Fig. 10 *A* illustrates calcium currents recorded in 2.6 mM Ca^{2+} with this technique. Inward currents are elicited at a threshold of about −50 mV, are maximal around −10 mV, and then decrease in amplitude with further depolarization, finally reversing at potentials positive to +80 mV. As previously reported (Plant, 1988), the rate and extent of inactivation varies with the amplitude

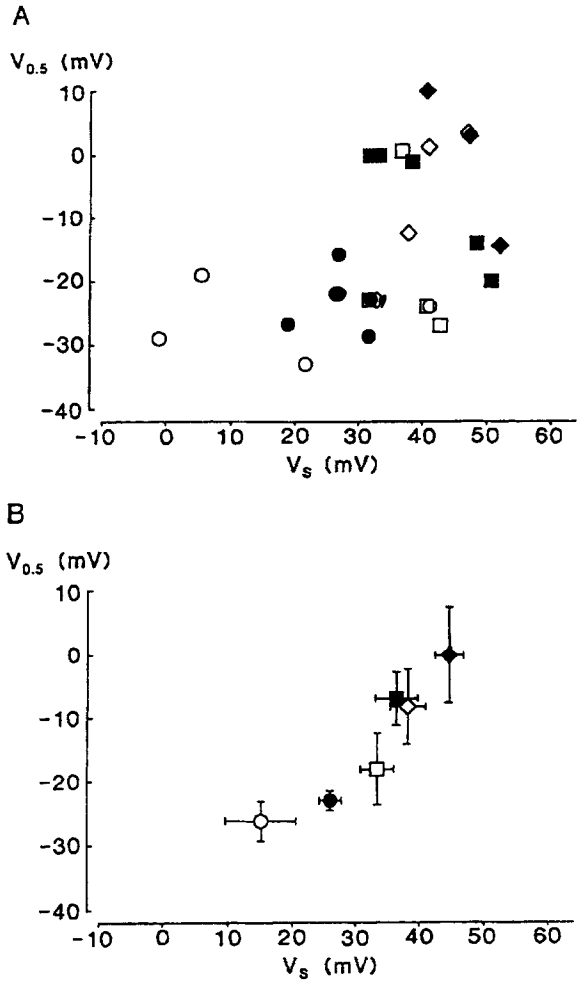

FIGURE 9. (*A*) Relationship between $V_{0.5}$ and V_s measured in the same patch. Each data point comes from a different patch. (○) 5 mM, (●) 10 mM, (□) 20 mM, (■) 40 mM, (◇) 70 mM, (◆) 100 mM Ba^{2+}. (*B*) Relationship between the mean value of $V_{0.5}$ and the mean value of V_s at different barium concentrations. (○) 5 mM (n = 4), (●) 10 mM (n = 7), (□) 20 mM (n = 4), (■) 40 mM (n = 5), (◇) 70 mM (n = 4), (◆) 100 mM (n = 3). Bars indicate ± SEM.

of the Ca^{2+} current, inactivation being greatest and most rapid when the Ca^{2+} currents are largest. Further evidence that inactivation is at least partly Ca^{2+} dependent is provided by the finding that the Ba^{2+} currents show much less inactivation (Fig. 10 *B*).

Fig. 10 *C* shows the associated whole-cell peak current–voltage relationship in 2.6 mM Ca^{2+} and 10 mM Ba^{2+}. There is little difference in the voltage dependence of

the current–voltage relation in these two solutions, suggesting that substitution of 10 mM Ba^{2+} for 2.6 mM Ca^{2+} produces little shift in surface potential. Further support for this idea was obtained by comparing the voltage dependence of channel activation (NP_o) in these two solutions. One method of determining NP_o is to divide the macroscopic current (I) by the measured value of the single channel current (i), as we did for the ensemble currents. An alternative approach, however, is to fit the peak current–voltage relationship directly with Eq. 11 (see below), which is derived by substituting Eqs. 1 and 8 in Eq. 7 (see also Markwardt and Nilius, 1988, who have used a similar approach). This approach is more suitable when the value of i cannot

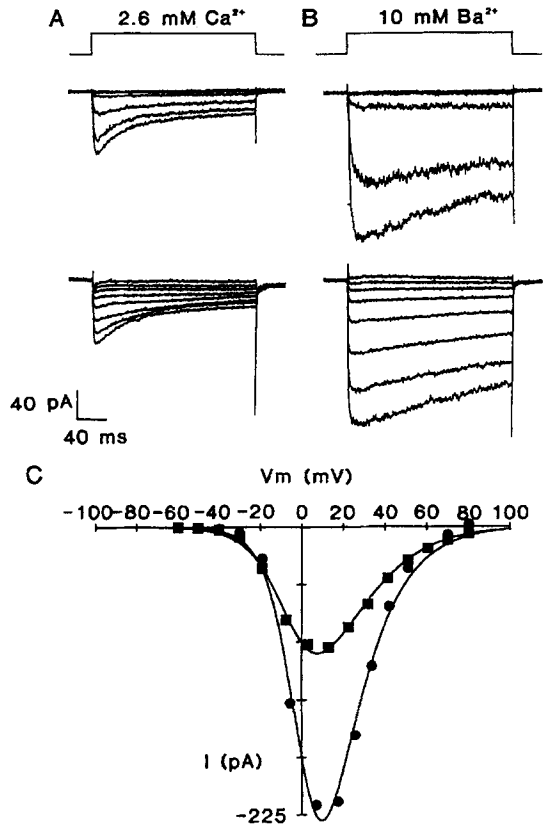

FIGURE 10. Whole-cell currents recorded in 2.6 mM Ca^{2+} (*A*) and subsequently in 10 mM Ba^{2+} (*B*). Currents were elicited by 250-ms pulses from a holding potential of −70 mV to potentials ranging between −60 and 0 mV (above) and between +10 and +80 mV (below) in 10-mV steps. (*C*) Peak current–voltage relations in 2.6 mM Ca^{2+} (■) and 10 mM Ba^{2+} (●). The lines are the best fits to Eq. 11.

be measured directly (as is the case in 2.6 mM Ca^{2+}). Eq. 11 states:

$$I = \frac{NP_{max}}{[1 + \exp[-(V - V_{0.5})/k]]^n} \frac{P_{Ba}(zF)^2 (V - V_s)}{RT} \cdot \exp(-zFV_s/RT) \frac{([Ba^{2+}]_o - [Ba^{2+}]_i \exp(zFV/RT)}{\{1 - \exp[zF(V - V_s)/RT]\}} \quad (11)$$

where I is the peak amplitude of the whole-cell inward current and other parameters

are defined as for Eqs. 1, 2, and 8. $[Ba^{2+}]_i$ was assumed to be zero and both the possibility of an outward Cs^+ current through the L-type calcium channel and any contribution of $[Ca^{2+}]_i$ were ignored (Wilson et al., 1983). As N, P_{max}, and P_{Ba} are interdependent, they were lumped together as a single value, $P_{Ba(max)}$, the maximum whole-cell barium permeability. V_s was taken as a free parameter, rather than as the value calculated from the single-channel current–voltage relation because of the different ionic conditions used in the whole-cell experiments. Although an outward current component was often present at positive potentials, producing an apparent reversal potential, this had little effect on the values obtained for k and $V_{0.5}$ (using Eq. 11). Whether n was taken as 1 or 2 had little effect on the overall closeness of fit, and n was thus fixed at 1. The lines in Fig. 10 *C* show representative fits of the peak whole-cell current voltage relations to Eq. 11.

The mean value of k in 10 mM Ba^{2+} was +7.6 ± 0.3 mV (n = 8), and is in good agreement with that obtained from our analysis of the ensemble Ba^{2+} currents (7.9 mV; Table II). The value of k in 2.6 mM Ca^{2+} was +8.4 ± 0.6 mV (n = 15), close to that found in barium (P = 0.63, paired).

The mean values of $V_{0.5}$ were −3.8 ± 1.3 mV (n = 15) in 2.6 mM Ca^{2+} and +3.5 ± 1.9 mV (n = 8) in 10 mM Ba^{2+}. The difference of 7.3 mV in the mean value of $V_{0.5}$ is similar to that of 8 mV estimated from the ensemble currents in calcium and barium solutions. Somewhat surprisingly, $V_{0.5}$ was 15–25 mV more negative in cell-attached patch studies (Table II) than in the whole-cell experiments for reasons that are unclear. This difference is unlikely to result from the 1.1 mM Mg^{2+} in the solution used for the whole-cell experiments since whole-cell calcium or barium currents were indistinguishable in the presence or absence of Mg^{2+}. Another explanation we have considered is that the difference in $V_{0.5}$ arises from our use of Cs^+ as a K^+ substitute in the pipette solution for the whole-cell experiments. In conventional whole-cell recordings of L-type Ca^{2+} currents, Malecot, Feindt, and Trautwein (1988) have shown that $V_{0.5}$ is 11 mV more positive when Cs^+ is used as a K^+ substitute rather than when *N*-methyl-glucamine (NMG) is used. A much larger shift appears to occur in β cells since the voltage dependence of the whole-cell current–voltage relation in 10 mM Ba^{2+}, recorded with NMG as the main intracellular cation (Plant, 1988), is ~30 mV more negative than that which we found using Cs^+; it is, however, remarkably similar to the ensemble current–voltage relation we record.

To test whether Cs^+ produces a shift in the voltage dependence of Ca^{2+} channel activation, whole-cell barium currents were measured with the perforated-patch technique, but using a K^+ nystatin solution in the pipette (Table I). The whole-cell barium currents measured using the K^+ solution were almost identical to those measured with Cs^+ solution (data not shown): the values of k and $V_{0.5}$ determined from fits of Eq. 11 to the peak current were similar to those obtained with a Cs^+ pipette solution (k = +7.3 compared with +7.6 ± 0.3 mV and $V_{0.5}$ = +3.4 mV compared with +3.5 ± 1.9 mV, for K^+ [n = 2] and Cs^+ [n = 8], respectively). However, the values of V_s were different, being +14 mV (n = 2) with K^+ as the internal cation and +4.5 ± 5 mV (n = 8) with Cs^+.

V_s was also affected by the external divalent cation, being −7.9 ± 2 mV (n = 15) in 2.6 mM Ca^{2+} and +4.5 ± 5 mV (n = 8) in 10 mM Ba^{2+} (P = 0.63, paired). This difference in V_s is similar to that estimated for the cell-attached studies (Table II). In

both Ca^{2+} and Ba^{2+} solutions, the value of V_s found in the whole-cell experiments was ~20 mV more negative than that estimated for the cell-attached experiments (2.6 mM Ca^{2+}, V_s = +9.7 mV; 10 mM Ba^{2+}, V_s = +26 mV; Table II).

The values obtained for both $V_{0.5}$ and V_s in 10 mM barium from the whole-cell currents were thus very different from those measured for the single-channel currents (Table II). To determine whether this difference arose from our fitting procedures, we fitted the peak current–voltage relationship of the ensemble currents to Eq. 11. The values obtained for V_s, $V_{0.5}$, and k were not significantly different from those calculated using Eqs. 1, 2, and 8 ($P > 0.2$, $n = 12$). Furthermore, although Eq. 11 has four free parameters, fixing the value of V_s had little effect on the calculated values of k and $V_{0.5}$; a +20-mV change in V_s produced a <5-mV change in $V_{0.5}$ and a <7% change in k.

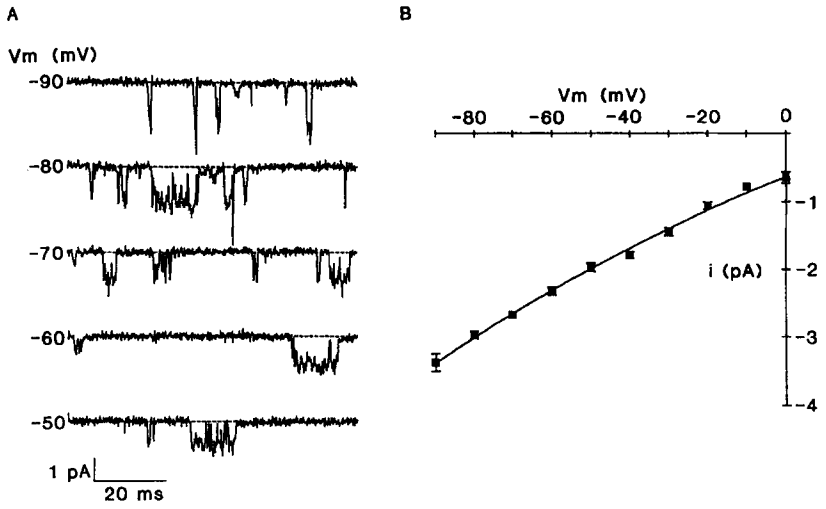

FIGURE 11. (*A*) Single-channel currents recorded in the absence of divalent cations with 150 mM Na^+ solution in the pipette. Currents were elicited by a 200-ms step to potentials indicated from a holding potential of −100 mV. Filter frequency, 2 kHz. (*B*) Single-channel current–voltage relationship for the channel shown in *A*. The line through the data points is the best fit to Eq. 1 with $P_{Na} = 1.4 \times 10^{-13}$ cm^3s^{-1} and V_s = +15 mV.

Permeation and Gating in the Absence of Divalent Cations; Na^+ Currents through L-Type Ca^{2+} Channels

Permeation. Na^+ currents through single L-type Ca^{2+} channels were recorded in the absence of extracellular divalent cations (Fig. 11 *A*). Addition of 20 μM nifedipine to the extracellular solution completely abolished these channel openings, confirming that they were due to the opening of L-type Ca^{2+} channels and not sodium channels (not shown, $n = 5$). Furthermore, the currents were unaffected by the addition of 1 μM tetrodotoxin to the pipette solution (not shown). Fig. 11 *B* shows the single Ca^{2+} channel current–voltage relation obtained with Na^+ as the charge carrier. The best fit

to Eq. 1 is shown as the solid line. Mean values were $1.0 \pm 0.2 \times 10^{-13}$ cm^3s^{-1} for the Na^+ permeability, P_{Na}; $+3.6 \pm 5$ mV for the voltage shift, V_s ($n = 5$); and 37 ± 5 mM for the internal Na^+ concentration (which is close to that found experimentally in the β cell, 36 mM; Smith, 1988). The single-channel slope conductance at −70 mV was 43 ± 3 pS ($n = 5$).

The very small voltage shift (V_s) observed in the absence of divalent cations indicates that Na^+ binds far less tightly to membrane surface charges than either Ba^{2+} or Ca^{2+}. If we assume that both the initial surface charge density ($\sigma_{(p)}$) and the internal surface potential ($\psi_{i(p)}$) are the same in Na^+ and Ba^{2+} solutions, that is, $\sigma_{(p)}$ is 1.4 $e.nm^{-2}$ and $\psi_{i(p)}$ is −51.1 mV, we calculate a dissociation constant ($K_{d(p)}$) for sodium of 336 mM ($K_{a(p)} = 3.0$ M^{-1}) (Table II). This value is much higher than that found for either calcium (18 mM) or barium (13 mM), suggesting that Na^+ binds only weakly to membrane surface charge associated with the mouth of the pore.

Gating. Ensemble currents constructed from the single-channel data obtained in Na^+ solution are shown in Fig. 12 *A* and the corresponding peak ensemble current–voltage relation in Fig. 12 *B*. Na^+ currents are elicited at around −100 mV and are maximal at −40 mV. These values are in good agreement with those reported for whole-cell Na^+ currents and are 20–30 mV more negative than those found in 10 mM Ba^+ solution (Plant, 1988). Unlike the whole-cell currents measured by Plant (1988), the ensemble Na^+ currents inactivated very rapidly, as expected since the single-channel currents were clustered toward the beginning of the trace (not shown). The voltage dependence of NP_o (Fig. 12 *C*) was determined for the ensemble Na^+ currents using the same method as described for the ensemble Ba^{2+} currents. The relationship was fit by Eq. 8 and gave mean values of $+7.5 \pm 1.1$ mV ($n = 3$) for k, and of -44 ± 4 mV ($n = 5$) for $V_{0.5}$. The value for $V_{0.5}$ is 21 mV more negative than that found in 10 mM Ba^{2+}; this difference is similar to that observed for V_s (23 mV; see above). Our results therefore indicate that removal of divalent cations produces a large negative shift in both $V_{0.5}$ and V_s (Table II).

In fitting the barium dependence of V_s and $V_{0.5}$ in Figs. 3 and 8 we did not include the data obtained in divalent cation-free solution. However, it is clear from Fig. 8 that the value of $V_{0.5}$ obtained in divalent cation-free solution is close to that predicted from the fitted relationship for zero barium. In the absence of divalent cations, it is also possible to obtain $\sigma_{(g)}$ from the Gouy expression, which assumes that ions screen, but do not bind to, membrane surface charge (McLaughlin et al., 1971). If we assume that $(B - \psi_{i(g)})$ is −20 mV (i.e., independent of the extracellular cation), we obtain a value of 0.5 $e.nm^{-2}$ for the initial surface charge density, $\sigma_{(g)}$. This value is close to that of 0.54 $e.nm^{-2}$ found for the best fit of Eq. 2 to the barium dependence of $V_{0.5}$, consistent with the idea that Na^+ does not readily bind to membrane surface charges associated with Ca^{2+} channel gating.

Effect of BAY-K 8644 on the Permeation and Gating Properties

BAY-K 8644 has been reported to exert part of its agonistic effect on the L-type calcium channel by shifting the voltage dependence of channel gating to more negative membrane potentials (Hess, Lansman, and Tsien, 1984; Sanguinetti, Krafte, and Kass, 1986; Markwardt and Nilius, 1988; Cena et al., 1989). It has been suggested that this may result from the drug interacting with membrane surface

charge in the vicinity of the gating particle (Kass and Krafte, 1987). As BAY-K 8644 has been used throughout this study, we examined its effect on the channel permeation and gating properties in 10 mM Ba^{2+} solution.

In cell-attached studies there was no effect of 0.1 μM BAY-K 8644 on the single-channel current–voltage relationship for the L-type calcium channel. There was also no consistent effect on V_s when the concentration of BAY-K 8644 was

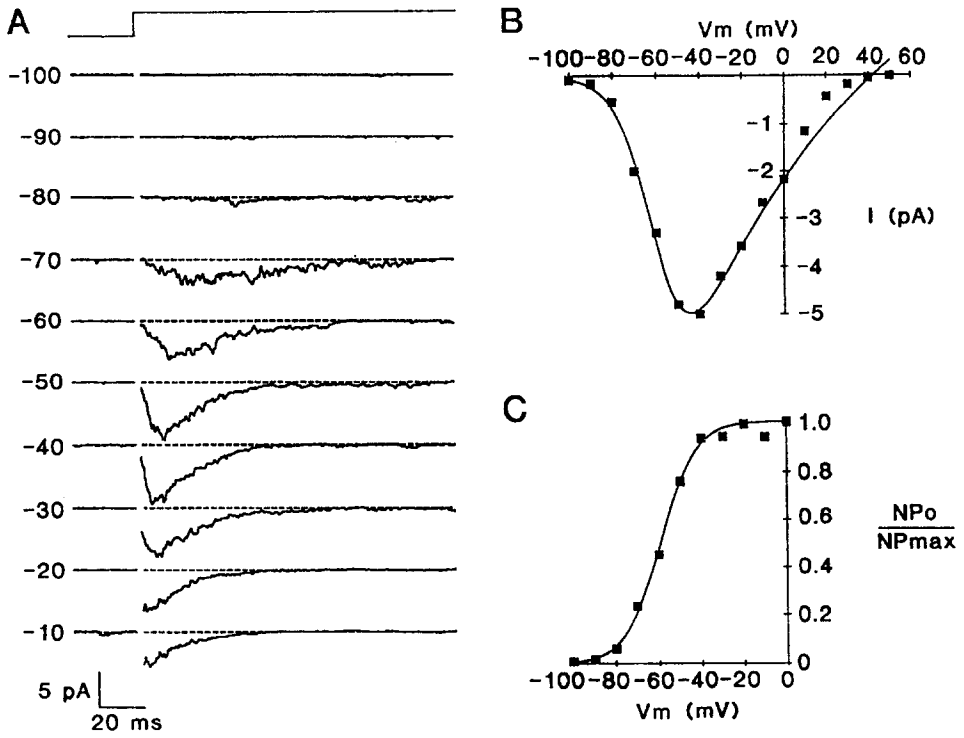

FIGURE 12. (*A*) Ensemble average currents recorded in 150 mM Na^+ solution from the same patch as in Fig. 11. Currents were elicited by a 200-ms step to indicated potentials from a holding potential of −100 mV. The pulse protocol is shown above. Filter frequency 0.5 kHz. Capacity transients have been omitted for clarity. (*B*) Peak ensemble current–voltage relationship for the patch shown in *A*. The line is the best fit to Eq. 11 using: k = 8.1 mV, $V_{0.5}$ = −59 mV, and V_s = +12 mV. (*C*) Normalized channel activity (NP_o/NP_{max}) as a function of membrane potential (V_m) in 150 mM Na^+ solution. The line is a fit to Eq. 8 using the same values as above. A similar fit was obtained when $V_{0.5}$, determined from Eq. 9, was set at −54 mV with a k of 8 mV. Same data as in *A*.

increased from 0.1 to 1 μM (P = 0.29). Mean values of V_s were +30 ± 2.6 mV (n = 5) in 0.1 μM BAY-K 8644 and +26 ± 2 mV after changing to 1 μM, with some patches showing an increase, and others no change or a decrease in V_s. Both the single-channel permeability and conductance were also little affected, changing from 8.5 ± 1 × 10^{-13} to 7 ± 1 × 10^{-13} cm^3s^{-1} (P = 0.59) and from 12.4 ± 1.4 to 13.6 ± 1.0 pS (P = 0.27), respectively, on increasing the drug concentration (n = 5). In several

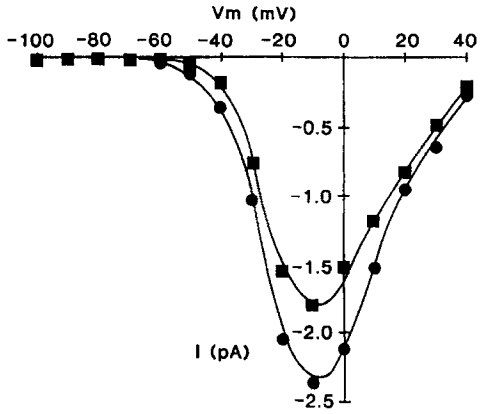

FIGURE 13. Ensemble peak current–voltage relationships measured with 10 mM Ba^{2+} in the pipette, in the presence of 0.1 μM BAY-K 8644 (■) and subsequently after increasing BAY-K 8644 to 1 μM (●).

patches showing high channel activity, it was possible to construct the ensemble peak current–voltage relationship at both BAY-K 8644 concentrations (Fig. 13). Raising BAY-K 8644 to 1 μM increased the ensemble current amplitude but did not alter the voltage dependence of the current–voltage relation. Thus the data strongly suggest

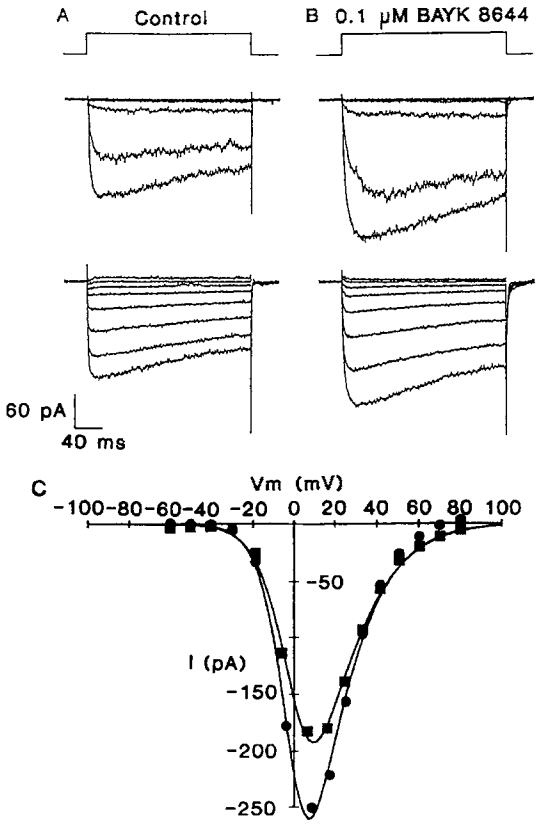

FIGURE 14. Whole-cell currents recorded in 10 mM Ba^{2+} in the absence (*A*) and subsequently the presence (*B*) of 0.1 μM BAY-K 8644. Currents were elicited by 250-ms pulses from a holding potential of −70 mV to potentials ranging between −60 and 0 mV (above) and between +10 and +80 mV (below) in 10-mV steps. (*C*) Peak current–voltage relations in the absence (■) and subsequently the presence (●) of 0.1 μM BAY-K 8644. Lines through the data are the best fit to Eq. 11.

that BAY-K 8644 itself does not induce a voltage shift in either the permeation or gating of L-type Ca^{2+} channels in mouse β cells.

The effect of BAY-K 8644 on the whole-cell currents was examined in 10 mM Ba^{2+} (Fig. 14, *A* and *B*). Addition of 0.1 μM BAY-K 8644 to the extracellular solution produced a small increase in current amplitude but did not shift the voltage dependence of the current–voltage relation (Fig. 14 *C*). Increasing the dihydropyridine concentration to 1 μM had similar effects (not shown). These results contrast with earlier reports showing that BAY-K 8644 induces a negative shift in the whole-cell current–voltage relationship of mouse β cells, measured with the standard whole-cell configuration (Plant, 1988; Rorsman et al., 1988).

Activation parameters were determined by fitting Eq. 15 to the peak current–voltage relationship. Neither $V_{0.5}$ nor k was significantly altered in the presence of the dihydropyridine agonist ($n = 6$): $V_{0.5} = +8.62 \pm 4.5$ mV and $k = +6.7 \pm 0.4$ mV in 0.1 μM BAY-K 8644; $V_{0.5} = +7.2 \pm 4.3$ mV and $k = +7.6 \pm 0.3$ mV in the absence of the drug ($P = 0.75$ and 0.14, respectively). As expected, V_s was also unaffected by BAY-K 8644 ($+6.6 \pm 2.8$ and $+7.7 \pm 3.8$ mV in the absence and presence of the drug, respectively; $P = 1.0$).

DISCUSSION

Surface Charge

Variations in the extracellular divalent cation concentration produced shifts in the voltage dependence of both the single-channel current–voltage relation and Ca^{2+} channel gating. We believe that these shifts arise from divalent cations interacting with membrane surface charges. It was not possible to fit the voltage shift in the single-channel current–voltage relation produced by varying $[Ba^{2+}]_o$ by assuming that divalent cations merely screen membrane surface charges (Fig. 3). Although a reasonable fit was obtained with binding alone, the best fit was achieved by allowing $[Ba^{2+}]_o$ to both bind to, and screen, membrane surface charge. Assuming both binding and screening, we calculate a value of 1.4 e.nm^{-2} for membrane surface charge associated with the ion permeation pathway ($\sigma_{(p)}$) and a $K_{d(p)}$ of 13 mM, the dissociation constant for Ba^{2+} binding to surface charge associated with the permeation pathway. A value of −51 mV was obtained for $\psi_{i(p)}$, the internal surface potential sensed by the permeation pathway. No values for these parameters have been reported previously.

The corresponding values for $\sigma_{(g)}$ and $K_{d(g)}$ associated with channel gating were very different: 0.54 e.nm^{-2} and 430 mM (for barium), respectively. Thus, although it has often been assumed that membrane surface charge sensed by the gating particle is the same as that sensed by the permeation pathway (Wilson et al., 1983; Cota and Stefani, 1984; Byerly, Chase, and Stimers, 1985; Ganitkevich et al., 1988), our measurements suggest that this is not true for the L-type Ca^{2+} channel of mouse β cells. Several studies have demonstrated that ion permeation through the channel is not influenced by the surface charge of the neighboring lipid environment (for example: Coronado and Affolter, 1986; Worley, French, Pailthorpe, and Krueger, 1992), which suggests that the mouth of the pore is effectively insulated from the lipid by both the bulk and structure of the channel protein. It seems likely that in

mouse β cells also the surface charge associated with permeation resides on the Ca^{2+} channel protein itself.

Values similar to those we obtained for the surface charge associated with calcium channel gating ($\sigma_{(g)}$) have been reported in other tissues: 0.2 $e.nm^{-2}$ in frog skeletal muscle (Cota and Stefani, 1984); 0.5 $e.nm^{-2}$ in guinea pig *Taenia coli* (Ganitkevich et al., 1988); 0.4 $e.nm^{-2}$ in cardiac myocytes (Kass and Krafte, 1987); and 0.5 $e.nm^{-2}$ in neurons of *Lymnea stagnalis* (Byerly et al., 1985). These values are lower than that of 2.6 $e.nm^{-2}$ associated with a bilayer composed solely of negatively charged lipids (McLaughlin et al., 1971), which suggests that either the gating particle is some distance from the membrane lipid, that a large proportion of the membrane near the gating particle consists of neutral lipids, or that the surface charge sensed by the gating particle is located on the channel protein itself.

The value of 430 mM that we determined for $K_{d(g)}$, the dissociation constant for barium binding to surface charge associated with channel gating, compares with that of 182 mM ($K_{a(g)}$ = 5.5 M^{-1}) reported for Ca^{2+} channels in smooth muscle (Ganitkevich et al., 1988). In other studies, binding of Ba^{2+} appears to be negligible (Cota and Stefani, 1984; Kass and Krafte, 1987). Our value for $K_{d(g)}$ for calcium (38 mM) lies well within the range observed in other tissues: 22 mM to 1 M (Cota and Stefani, 1984; Kass and Krafte, 1987; Ganitkevich et al., 1988).

There does not appear to be a direct correlation between V_s and $V_{0.5}$ even in the same patch (Fig. 9). Plotting the mean values for V_s and $V_{0.5}$ for each concentration of barium does suggest some form of correlation, however, as is expected if both variables depend on the concentration of barium (Fig. 9).

Conductance and Permeability

The saturation of the single-channel conductance at high $[Ba^{2+}]_o$ can be attributed to Ba^{2+} screening, and binding to, membrane surface charge in the vicinity of the channel mouth. This explains why the conductance shows little saturation when expressed as a function of the surface Ba^{2+} concentration. It also indicates that the affinity of the ion-binding site within the pore is substantially overestimated when the effect of surface charge is ignored ($K_{d(\gamma)}$ = 200 mM, as opposed to 5.5 mM when the bulk Ba^{2+} concentration is used). After correction for surface charge, it is apparent that there is no substantial binding of Ba^{2+} to sites within the pore. Since different ionic species may vary in their ability to bind to surface charge, thus producing different surface concentrations, the true permeability sequence of the channel may differ from that calculated using the bulk concentration of the ion. For the L-type Ca^{2+} channel in mouse β cells, the true permeability sequence is $Na^+ = Ba^{2+} > Ca^{2+}$ (Table II).

Values for $K_{d(\gamma)}$ of 8–13 mM, calculated using the bulk barium concentration, have been obtained for single L-type Ca^{2+} channels in other preparations (Rosenberg et al., 1988; Ganitkevich and Isenberg, 1990), and compare favorably with that reported here (5.5 mM). However, as discussed by Yue and Marban (1990), when plotted as a function of $[Ba^{2+}]_o$, the data are poorly fitted by a Langmuir saturation curve, the conductance continuing to increase (creep) at higher barium concentrations (Fig. 4 *A*).

A number of models of varying complexity have sought to describe ion permeation

through the Ca^{2+} channel. To account for the saturation of the conductance, all of these models assume that ions bind within the pore as they pass through it. The simplest model assumes a single binding site (Ashcroft and Stanfield, 1982). This model, however, cannot easily account for all of the reported properties of the L-type Ca^{2+} channel; for example, the anomalous mole-fraction effect, the dramatic increase in monovalent ion permeability when divalent cations are removed, and the creep in the conductance–concentration relationship. To explain these properties, two main approaches have been developed: these assume either the presence of multiple binding sites within the pore (Almers and McClesky, 1984; Hess and Tsien, 1984) or the existence of an extracellular divalent cation binding site (Hagiwara and Takahashi, 1967; Kostyuk, Mironov, and Shuba, 1983). Yue and Marban (1990), have shown that the anomalous mole-fraction effect does not occur at the single-channel level in cardiac myocytes, but they still favor a multi-ion occupancy model because of the creep in the conductance–concentration relationship. Conversely, Armstrong and Neyton (1991) have proposed a single ion-binding site model for ion permeation through the calcium channel. Their model, however, cannot account for the creep in the concentration–conductance curve. Our data show that this creep may be the consequence of ion binding to membrane surface charge. This implies that multi-ion pore models may not be necessary to explain permeation through the L-type Ca^{2+} channel (Armstrong and Neyton, 1991) and also emphasizes that it is important to consider the effects of surface charge when formulating models of ion permeation. Our data also suggest that the GHK-model of ion-permeation can adequately describe ion permeation through the L-type calcium channel under a limited set of conditions.

Effect of the Dihydropyridine, BAY-K 8644

In both the cell-attached and the perforated-patch experiments, BAY-K 8644 had no effect on either the single-channel current amplitude or the voltage dependence of activation. The lack of an effect on the single-channel conductance is well established (Hess et al., 1984; Fox et al., 1987). What is surprising is our finding that BAY-K 8644 did not shift the voltage dependence of activation. This is in contrast to other tissues, where the drug produces a negative shift in the voltage-dependence of L-type Ca^{2+} channel activation (Hess et al., 1984; Fox et al., 1987; Sanguinetti et al., 1986). Furthermore, previous studies in mouse β cells have also reported a negative shift in the whole-cell Ca^{2+} current–voltage relationship with dihydropyridine agonists (1 μM BAY-K 8644, Rorsman et al., 1988; 5 μM CGP 28392, Plant, 1988).

The main differences between our whole-cell studies and earlier work on β cells is that we used the perforated-patch rather than the conventional whole-cell recording configuration, and Cs^+ rather than *N*-methyl-glucamine (NMG^+) as a K^+ substitute in the pipette. We also saw no effect of BAY-K 8644 on the voltage dependence of gating in cell-attached patches. In both the cell-attached and perforated-patch configurations the cell is intact and loss of cytosolic constituents is minimized. One possible explanation for the shift in the voltage-dependence of the current–voltage relation induced by BAY-K 8644 in conventional whole-cell studies, therefore, is that it results from the loss of some cytoplasmic factor.

Activation

Both $V_{0.5}$ and the potential at which the maximum current occurred were ~30 mV more positive for the whole-cell current than for the ensemble current in 10 mM Ba^{2+}. One possible reason for this difference is the presence of a Donnan potential across the perforated-patch membrane, although this seems unlikely since Donnan potentials should be small with the pipette solutions we used (Horn and Marty, 1988). Another possible source of error that can be dismissed is that the resting membrane potential was not actually 0 mV, as we assumed; in separate experiments we measured the resting potential as +5 mV and correction for this error would have the effect of increasing the difference in $V_{0.5}$ to +35 mV. There appears to be no difference when K^+ or Cs^+ is used in the pipette for perforated-patch whole-cell recording of calcium currents; thus the use of Cs^+ as an internal cation does not account for the difference between cell-attached and perforated-patch studies, or for that between perforated-patch and previous whole-cell studies. The reasons behind the differences in the values of $V_{0.5}$ and V_s from cell-attached and perforated-patch whole-cell studies therefore remain unresolved, although it seems to relate to the use of the perforated-patch recording configuration. Whether NMG is a more suitable K^+ substitute than Cs^+ for standard whole-cell recordings also remains to be ascertained.

The difference in $V_{0.5}$, the voltage dependence of gating, that we observed for the ensemble currents in 100 mM and 10 mM Ba^{2+} is about +22 mV, and the difference between $V_{0.5}$ for the whole-cell currents recorded in 10 mM Ba^{2+} and 2.6 mM Ca^{2+} is +8 mV. This suggests that in mouse pancreatic β cells there is a positive shift in the activation curve of L-type Ca^{2+} channel gating of ~30 mV between 2.6 mM Ca^{2+} and 100 mM Ba^{2+}.

Inactivation

The more rapid inactivation of single-channel Ca^{2+} currents, as compared with single-channel Ba^{2+} currents, suggests that Ca^{2+}-dependent inactivation may occur in cell-attached patches. This finding is in agreement with that of Yue, Backx, and Imredy (1990), who used conditional open probability analysis to demonstrate Ca^{2+}-dependent inactivation at the single-channel level in cardiac myocytes. In common with earlier studies, a slow inactivation of the ensemble Ba^{2+} currents was also observed. Whether this reflects an ability of Ba^{2+} to substitute for Ca^{2+} in the inactivation process or whether it represents a component of voltage-dependent inactivation is unknown. The inactivation of the ensemble Na^+ currents, a phenomenon we also observed in perforated-patch recordings, was not found in conventional whole-cell studies (Plant, 1988). This difference may result from dialysis of the cell cytoplasm in Plant's studies since we observed inactivation of whole-cell Na^+ currents in perforated-patch recordings (data not shown).

Physiological Implications

Most previous studies of single Ca^{2+} channel currents have been carried out using 100 mM Ba^{2+} as the charge carrier to increase the current amplitude, and using BAY-K 8644 to prolong the channel lifetime. These conditions are far from physiological. In mouse β cells, we have found that BAY-K 8644 has little effect on

the voltage dependence of channel activation. However, the high divalent cation concentration produces a shift in activation to potentials that are considerably more depolarized than those found in a more physiological saline solution containing 2.6 mM Ca^{2+}. A much smaller shift was found, however, when the charge carrier was 10 mM Ba^{2+}. Since single-channel currents can still be resolved quite easily in 10 mM Ba^{2+}, this would appear to be an appropriate experimental solution.

In 10 mM Ba^{2+}, single-channel activity is seen at, or more negative to, the β cell resting potential (−70 mV). This suggests that Ca^{2+} influx through L-type Ca^{2+} channels may contribute to the background Ca^{2+} influx into the β cell and would explain why dihydropyridine agonists can increase (Malaisse-Lagae, Mathias, and Malaisse, 1984; Boschero, Carrol, DeSouza, and Atwater, 1990) and dihydropyridine antagonists decrease (Al-Mahood, El-Khatim, Gumaa, and Thulesius, 1986) basal insulin secretion.

We thank the British Diabetic Association, the Wellcome Trust, and the Royal Society for support. F.M. Ashcroft was a Royal Society 1983 University Research Fellow. C.M.S. Fewtrell was an NIH Senior Fellow.

Original version received 19 May 1992 and accepted version received 30 November 1992.

REFERENCES

Al-Mahood, H. A., M. S. El-Khatim, K. A. Gumaa, and O. Thulesius. 1986. The effect of calcium blockers nicardipine, darodipine, PN-200-110 and nifedipine on insulin release from isolated rat pancreatic islets. *Acta Physiologica Scandinavica.* 126:295–298.

Almers, W., and E. W. McCleskey. 1984. Non-selective conductance in calcium channels of frog muscle: calcium selectivity in single file pore. *Journal of Physiology.* 353:585–608.

Armstrong, D. L., and J. Neyton. 1991. Ion permeation through calcium channels: a one site model. *Annals of the New York Academy of Sciences.* 635:18–25.

Ashcroft, F. M., R. P. Kelly, and P. A. Smith. 1990. Two types of Ca channel in rat pancreatic B-cells. *Pflügers Archiv.* 415:504–506.

Ashcroft, F. M., and P. Rorsman. 1989. Electrophysiology of the pancreatic β-cell. *Progress in Biophysics and Molecular Biology.* 87–144.

Ashcroft, F. M., and P. R. Stanfield. 1982. Calcium and potassium currents in muscle fibres of an insect (*Carausius Morosus*). *Journal of Physiology.* 323:93–115.

Atwell, D., and D. Eisner. 1978. Discrete membrane surface charge distributions. *Biophysical Journal.* 24:869–875.

Bokvist, K., P. Rorsman, and P. A. Smith. 1990*a*. Effects of external tetraethylammonium ions and quinine on delayed rectifying K-channels in mouse pancreatic B-cells. *Journal of Physiology.* 423:311–325.

Bokvist, K., P. Rorsman, and P. A. Smith. 1990*b*. Block of ATP-regulated and Ca^{2+}-activated K-channels in mouse pancreatic B-cells by external tetraethylammonium and quinine. *Journal of Physiology.* 423:327–342.

Boschero, A. C., P. B. Carrol, C. DeSouza, and I. Atwater. 1990. Effects of Ca^{2+} channel agonist-antagonist enantiomers of dihydropyridine 202791 on insulin release, $^{45}Ca^{2+}$ uptake and electrical activity in isolated pancreatic islets. *Experimental Physiology.* 75:547–558.

Byerly, L., P. B. Chase, and J. R. Stimers. 1985. Permeation and interaction of divalent cations in calcium channels of snail neurons. *Journal of General Physiology.* 85:491–518.

Cena, V., A. Stutzin, and E. Rojas. 1989. Effects of calcium and BAY K 8644 on calcium currents in adrenal medullary chromaffin cells. *Journal of Membrane Biology.* 112:255–265.

Coronado, R., and H. Affolter. 1986. Insulation of the conduction pathway of muscle transverse tubule calcium channels from the surface charge of bilayer phospholipid. *Journal of General Physiology.* 87:933–953.

Cota, G., and E. Stefani. 1984. Saturation of calcium channels and surface charge effects in skeletal muscle fibres of the frog. *Journal of Physiology.* 351:135–154.

Fox, A. P., M. C. Nowycky, and R. W. Tsien. 1987. Single-channel recordings of three types of calcium channels in chick sensory neurones. *Journal of Physiology.* 394:173–200.

Frankenhaeuser, B. 1960. Sodium permeability in toad nerve and in squid nerve. *Journal of Physiology.* 152:159–166.

Ganitkevich, V. Y., and G. Isenberg. 1990. Contribution of two types of calcium channels to membrane conductance of single myocytes from guinea-pig coronary artery. *Journal of Physiology.* 426:19–42.

Ganitkevich, V. Y., M. F. Shuba, and S. V. Smirnov. 1988. Saturation of calcium channels in single isolated smooth muscle cells of guinea-pig taenia caeci. *Journal of Physiology.* 399:419–436.

Goldman, D. E. 1943. Potential, impedance, and rectification in membranes. *Journal of General Physiology.* 27:37–60.

Hagiwara, S., and K. Takahashi. 1967. Surface density of calcium ions and calcium spikes in the barnacle muscle fiber membrane. *Journal of General Physiology.* 50:583–601.

Henquin, J. C., and H. P. Meissner. 1984. Significance of ionic fluxes and changes in membrane potential for stimulus-secretion coupling in pancreatic B-cells. *Experientia.* 40:1043–1052.

Hess, P., J. B. Lansman, and R. W. Tsien. 1984. Different modes of Ca channel gating behaviour favoured by dihydropyridine Ca agonists and antagonists. *Nature.* 311:538–544.

Hess, P., J. B. Lansman, and R. W. Tsien. 1986. Calcium channel selectivity for divalent and monovalent cations. *Journal of General Physiology.* 88:293–319.

Hess, P., and R. W. Tsien. 1984. Mechanism of ion permeation through calcium channels. *Nature.* 309:453–456.

Hodgkin, A. L., and B. Katz. 1949. The effects of sodium ions on the electrical activity of the giant axon of the squid. *Journal of Physiology.* 108:37–77.

Horn, R., and A. Marty. 1988. Muscarinic activation of ionic currents measured by a new whole-cell recording method. *Journal of General Physiology.* 92:145–159.

Kass, R. S., and D. S. Krafte. 1987. Negative surface charge density near heart calcium channels. *Journal of General Physiology.* 89:629–644.

Korn, S. J., and R. Horn. 1989. Influence of sodium-calcium exchange on calcium current rundown and the duration of calcium-dependent chloride currents in pituitary cells, studied with whole cell and perforated patch recording. *Journal of General Physiology.* 94:789–812.

Kostyuk, P. G., S. L. Mironov, and Y. M. Shuba. 1983. Two ion-selecting filters in the calcium channel of the somatic membrane of mollusc neurons. *Journal of Membrane Biology.* 76:83–93.

Malaisse-Lagae, F., P. C. F. Mathias, and W. J. Malaisse. 1984. Gating and blocking of calcium channels by dihydropyridines in the pancreatic B-cell. *Biochemical and Biophysical Research Communications.* 123:1062–1068.

Malecot, C. O., P. Feindt, and W. Trautwein. 1988. Intracellular N-methyl-D-glucamine modifies the kinetics and voltage-dependence of the calcium currents in guinea pig ventricular heart cells. *Pflügers Archiv.* 411:235–242.

Markwardt, F., and B. Nilius. 1988. Modulation of calcium channel currents in guinea-pig single ventricular heart cells by the dihydropyridine BAY K 8644. *Journal of Physiology.* 399:559–575.

McLaughlin, S. G. A., G. Szabo, and G. Eisenman. 1971. Divalent ions and the surface potential of charged phospholipid membranes. *Journal of General Physiology.* 58:667–687.

Plant, T. D. 1988. Properties and calcium-dependent inactivation of calcium currents in cultured mouse pancreatic B-cells. *Journal of Physiology.* 404:731–747.

Prentki, M., and F. M. Matschinsky. 1987. Ca^{2+}, cAMP, and phospholipid-derived messengers in coupling mechanisms of insulin secretion. *Physiological Reviews.* 67:1185–1249.

Rorsman, P., F. M. Ashcroft, and G. Trube. 1988. Single Ca channel currents in mouse pancreatic B-cells. *Pflügers Archiv.* 412:597–603.

Rorsman, P., and G. Trube. 1986. Calcium and delayed potassium currents in mouse pancreatic B-cells under voltage clamp control. *Journal of Physiology.* 374:531–550.

Rosenberg, R. L., P. Hess, and R. W. Tsien. 1988. Cardiac calcium channels in planar lipid bilayers. *Journal of General Physiology.* 92:27–54.

Sala, S., and D. R. Matteson. 1990. Single-channel recordings of two types of calcium channels in rat pancreatic B-cells. *Biophysical Journal.* 58:567–571.

Sanguinetti, M. C., D. S. Krafte, and R. S. Kass. 1986. Voltage-dependent modulation of Ca channel current in heart cells by BAY K 8644. *Journal of General Physiology.* 88:369–392.

Smith, P. A. 1988. Electrophysiology of B-cells from pancreatic islets of Langerhans. Ph.D thesis. University of East Anglia, Norwich, UK. 358 pp.

Smith, P. A., P. Rorsman, and F. M. Ashcroft. 1989. Modulation of dihydropyridine sensitive Ca^{2+} channels by glucose metabolism in mouse pancreatic B-cells. *Nature.* 342:550–553.

Wilson, D. L., K. Morimoto, Y. Tsuda, and A. M. Brown. 1983. Interaction between calcium ions and surface charge as it relates to calcium currents. *Journal of Membrane Biology.* 72:117–130.

Worley, J. F., R. J. French, B. A. Pailthorpe, and B. K. Krueger. 1992. Lipid surface charge does not influence the conductance or calcium block of single sodium channels in planar bilayers. *Biophysical Journal.* 61:1353–1363.

Yue, D. T., P. H. Backx, and J. P. Imredy. 1990. Calcium sensitive inactivation in the gating of single calcium channels. *Science.* 250:1735–1738.

Yue, D. T., and E. Marban. 1990. Permeation in the dihydropyridine-sensitive calcium channel. *Journal of General Physiology.* 95:911–939.